MASTER MEMORY

Material sciences
physics
Condensed Matter Physics

Réf.:

Prsentedd by:

DOUBA OUISSAL

Effect of Cesium doping on the properties of Titanium dioxide thin films elaborated by Sol- gel (Spin coating) and their photocatalytic applications.

Jury:

Nouadji Malika	MCA	University of Med Khider	President
Saidi Hanane	Pr	University of Med Khider	Reporter
Hamani Nadjette	MCB	University of Med Khider	Examiner

Academic Year: 2022/2023

Dedication

With the help of God, I was able to carry out this modest work, which I dedicate to my family.

It was my parents' unconditional love, care, and tolerance which made the hardship of writing the dissertation worthwhile. I am greatly indebted to my brothers and my sisters especially my sister Zahra and her husband, they both showed great support to me. I dedicate this work to my dear Leasa who was looking forward to my successful graduation.

Also, a big thank t o my friends: Khaoula, Remaissa, Ines, Chams and Noumidia.

Acknowledgments

Summary

Chapter 03: Experimental procedures, results and discussions

General introduction

In several domains, transparent and conductive oxides (TCO) are exceptional materials. They are excellent candidates for use in photovoltaic and optoelectronic applications due to their dual property of electrical conductivity and optical transparency. Through a variety of methods, including radio frequency magnetron sputtering (PMRF), pulsed laser deposition (PLD), jet pyrolysis (PS), sputtering, sol-gel technique, and the Spray pyrolysis process, these materials (TCO) were deposited in thin layers [1].

Titanium dioxide is a cheap, non-toxic material and has high chemical and mechanical stability. In addition, titanium dioxide has very good semiconductor properties, which has generated significant enthusiasm on the part of scientists for various applications, and in particular photo-catalysis, gas sensors, anti-reflective coatings, optical guides and optical waves. Several studies have been devoted to the doping of thin layers of TiO_2 obtained by the sol-gel process. The presence of impurities in a matrix can stabilize, improve or modify the various properties of a material. Generally, thin layers of doped TiO_2 give hope for significant performance gains, as well as new applications, because the size effect of dopants (nanocrystals, nanoparticles) strongly modify the different physico-chemical properties of TiO_2 [2,3].

This work focused on the development and characterization of titanium oxide doped with Cesium (TiO_2: Cs) in thin layers. The aim of this work is concerned with improving the structural, optical and electrical properties of TiO_2 thin films during Cesium doping for photocatalytic applications. The manuscript is composed of three chapters and a general conclusion.

In the first chapter we did a bibliographic research on transparent conductive oxides in general and we presented titanium dioxide, their properties and applications, then we talked about Cesium as a doping element.

In the second chapter, we presented a description of some different deposition processes, which makes it possible to obtain thin layers and we precisely the Sol-Gel technique (spin-coating). A description of the various characterization techniques used in this work is also given.

The third chapter is devoted to the experimental procedure of the preparation of the layers, and the discussion and interpretation of the results obtained.

References

[1] **A. Abdlekrim**, « Optimisation des conditions d'élaboration des couches minces d'oxyde d'étain SnO_2 par spray », thèse de doctorat, université de Biskra, (2016).

[2] **F. Medjaldi, A. Bouabellou**, « Préparation et caractérisation de couches minces d'oxyde de titane (TiO_2) et du couple d'oxydes (TiO_2/SnO_2) », mémoire de magister, université de Constantine, (2017).

[3] **R. Messemeche,** « Elaboration and characterization of undoped and doped titanium dioxide thin layers by sol gel (spin coating) for photocatalytic applications », thèse de doctorat, université de Biskra, (2021).

Chapter I

Generalities about Titanium dioxide

In this chapter, we presented a literature study about transparent conducting oxide (TCO), and in particular we focused on the most popular transparent conducting oxide that namely titanium dioxide (TiO_2). The brief and complete definition of TiO_2, as well as its properties and certain areas of application is been clarified.

I.1. Transparent conducting oxide (TCO)

I.1.1. Definition

Transparent conducting oxides (TCO) are electrically conductive materials with a relatively low amount of light absorption [1]. It is impossible for an intrinsically stoichiometric material to exhibit high optical transparency (more than 80% in the visible spectrum) and high electrical conductivity (about $10^3 \ \Omega^{-1} \ cm^{-1}$ or more) at the same time. Partial transparency and fairly good conductivity may be obtained in thin films of a variety of metals. The only way to obtain good transparent conductors is to create electron degeneracy in a wide band gap (greater than 3 eV) oxide by controllably introducing non-stoichiometry and/or appropriate dopants. These conditions are very conveniently obtained in oxides of cadmium, tin, indium, zinc and their alloys in thin film form, prepared by a number of deposition techniques [2].

I.1.2. Applications of TCO films

The properties of TCO demonstrated previously make it possible to envisage their use in numerous applications (Fig.I.1). The main uses of these materials are [3]:

- Flat screens.
- Frost protection window.
- Heat-reflecting window (building, oven, etc.).
- Electromagnetic protection.
- Solar cells: as a front contact through which light must pass in order to enter the cell.

For each application the TCO is chosen according to the manufacturing requirements and properties required for application.

Fig.I.1 Some application of TCO [4].

The preparation of transparent conducting oxide (TCO) thin layers for widespread use in the technological field of optoelectronic devices has attracted increasing interest in recent years. One of these outstanding, thoroughly researched transparent conducting oxide compounds with numerous uses in various fields is titanium oxide (TiO_2) [5].

I.2. Titanium Dioxide

I.2.1. Definition

Titanium dioxide belongs to the chemical family of transition metal oxides [6] and It is a n-type semiconductor with a wide indirect energy band gap [7]. It has a particularly high refractive index and its insensitivity to visible light, due to its wide indirect band gap (3.2 eV) only allows it to absorb in the near ultraviolet. It has a very high scattering coefficient for the visible light spectrum with no absorption zone [6], (see Fig.I.2).
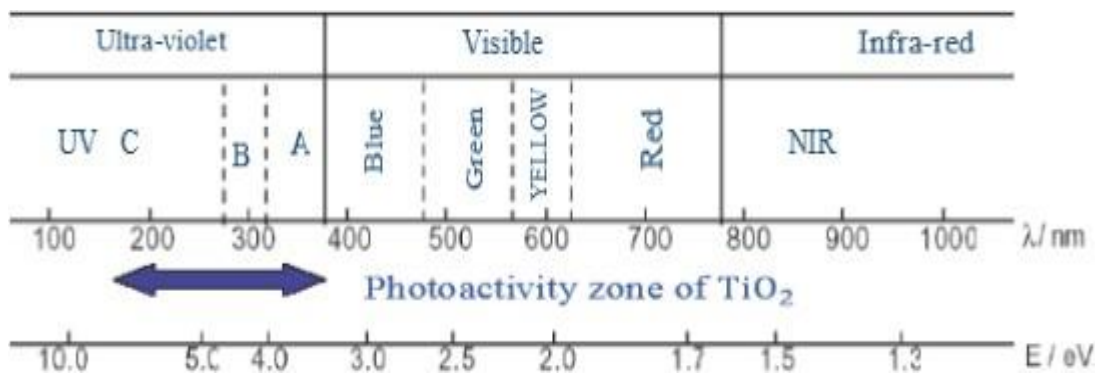
Fig.I.2 Spectrum of light with the action zone of TiO_2 [6].

Table.I.1 Characteristics of titanium dioxide in the macroscopic state [8,9].

IUPAC name	Titanium dioxide
Chemical formula	TiO_2
Molar mass	$79.890\ g.m^{-1}$
Volumetric mass	3.9 to 4.3 $g.cm^3$
Solubility	Insoluble in water/organic solvents
Melting temperature	1855°C
Atomic radius (nm)	0.146 nm for (Ti) 0.066 nm for (O)
Ionic radius (nm)	0.064 nm for (Ti^{+4}) 0.14 nm for (O^{-2})

I.2.2. Choice of Titanium dioxide

Titanium dioxide (TiO_2) is one of the most alluring materials for experimental study due to its significance in science and technology [9]. Due to its optical, physical, chemical, and electrical characteristics, such as their good visible light transmittance, photocatalytic activity, high dielectric constant, high refractive index, and high chemical stability, an inexpensive and non-toxic, titanium dioxide (TiO_2) thin films have received a lot of interest. These characteristics are highly influenced by TiO_2 's micro-/nanostructure and crystallinity [7].

I.2.3. Titanium Dioxide properties

I.2.3.1. Structural properties

As is well known, TiO_2 has three primary crystalline forms at atmospheric pressure: Brookite, Anatase and Rutile. Due to its instability, Brookite, one of three crystalline phases of TiO_2,is rarely used in real-world applications. In contrast, anatase and rutile have received the most research attention [10].

✓ **Rutile phase**

The rutile TiO_2 structure, whose unit cell is quadratic, is described as a compact hexagonal stack of oxygen atoms in which one out of two octahedral sites is occupied by a Ti^{+4} ion. In its stoichiometric form, the Bravais lattice is tetragonal and contains six atoms per cell. Its crystal parameters are a = 0.45937 nm and c = 0.29581 nm. It is the densest form of titanium

dioxide, stable at high temperatures and high pressures. When stoichiometric, rutile TiO_2 insulated with a band gap of about 3 eV. However, deviations from stoichiometry can be obtained by annealing at high temperature (> 500°C) under ultra-high vacuum or under a reducing atmosphere and by interaction with a beam of charged particles (electrons or ions). Point defects appearing either in the form of interstitial titanium ions (major defects in the case of low sub-stoichiometries), or in the form of oxygen vacancies are then created, which makes the oxide n type semi-conductor [11].
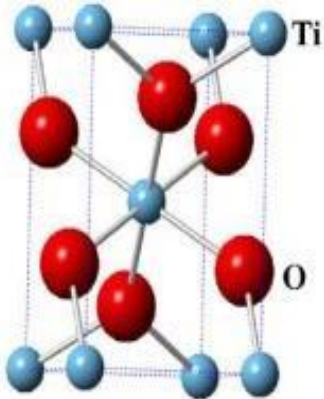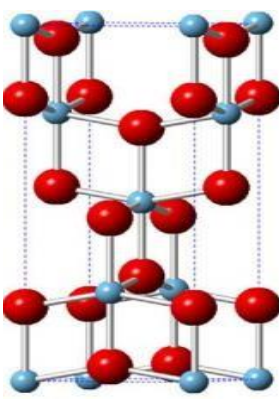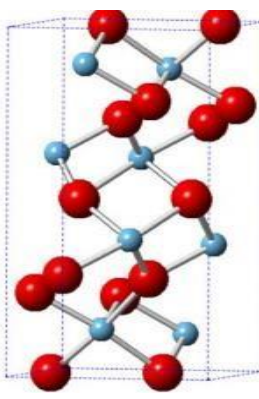
✓ **Brookite phase**

Brookite has a crystal structure of orthorhombic symmetry, of a D_{2h} symmetry group, it comprises eight molecules per cell. Its lattice parameters are: a = 0.54558 nm, b = 0.91819 nm and c = 0.51429 nm. This structure is more complex than the two other, more abundant phases (anatase and rutile). It is an intermediate phase of the transformation from anatase to rutile, it is also metastable [12]. Brookite transforms into rutile at high temperatures higher than 750°C. It shares almost the same properties as rutile, such as: color, hardness and density but it is less common and rarely used commercially [13].

✓ **Anatase phase**

It is a form of natural titanium oxide, which is encountered less frequently. It has a wide range of hues, from almost colorless to brown, passing through greenish. The unit cell of anatase is also of tetragonal symmetry with the parameters a = 3.7710 and c=9.430 whose ratio $^c/_a =$ 2.5134, except that the interatomic distances in the crystal are very slightly shortened compared to rutile: four short (1.933 Å) quasi-equatorial bonds and two long (1.978 Å) apical bonds for each titanium atom. Oxygen atoms are trivalent with two short bonds and one long bond [14].

Table.I.2 Crystal structure data of TiO$_2$ [15].			
Phase	**Rutile**	**Anatase**	**Brookite**
Crystal structure	Tetragonal	Tetragonal	orthorhombic
Lattice constants ($\mathring{A}$)	**a=4.594, c=2.958**	**a=3.784, c=9.515**	**a=9.182, b=9.19, c=5.143**
Molecule/cell	**2**	**4**	**8**
(Volume/molecule)($\mathring{A}^3$)	31.2160	34.061	32.172
Density(g/cm^3)	4.13	3.79	3.99
Ti-O bond length ($\mathring{A}$)	1.949 (4), 1.980 (2)	1.937 (4), 1.965 (2)	1.87~2.04

I.2.3.2. Optical properties

a. Refractive index

The refractive index n of the various types of titanium oxide is high in the visible range. Rutile has the greatest index (n $\sim$ 2.66) of the three stable crystalline phases, surpassing that of the anatase type (n $\sim$ 2.54). This makes the Rutile phase a popular white pigment for the industry, along with a high visible light scattering coefficient [16].

b. Optical gap

TiO$_2$ is described as having a large prohibited band (band-gap) and being a semiconductor material. Rutile, Anatase, and Brookite all have gaps that are 3 eV, 3.2 eV, and 3.1 eV, respectively. Between the valence band (which corresponds to the O 2p orbital) and the conduction band (which corresponds to the orbital Ti 3d), there is a band gap (Eg). These gap values result in transitions that correspond to ultraviolet-range photons. TiO$_2$'s transparency in the visible spectrum combined with an absorption edge around 0.42 μm causes a significant absorption in the ultraviolet, giving it exceptional qualities including UV radiation protection [17].

I.2.3.3. Electronic properties

Titanium dioxide is a semiconductor n type. The 2p orbitals of oxygen atoms dominate the energy levels at the top of the valence band (hence the notation P_π), whereas the 3d orbitals of titanium atoms dominate the energy levels at the bottom of the conduction band (hence the notation d). The interactions that shape the various chemical orbitals in anatase are detailed in figure.I.3. Dotted lines indicate weak contributions, whereas solid lines indicate substantial contributions [18], (see Fig.I.3).
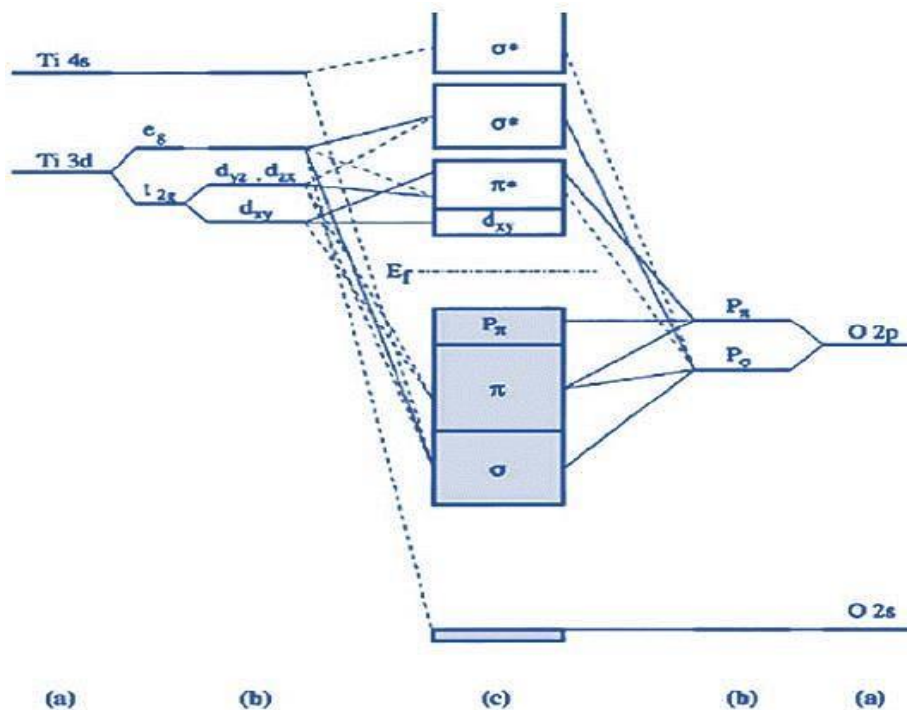
Fig.I.3 Schematic electronic structure of TiO$_2$ anatase, (a) atomic levels, (b) bursting of the levelsunder the effect of the crystalline field, (c) levels of interactions [18].

I.2.4. Non-Stoichiometric TiO_{2-x} Thin Films

The semiconducting properties of non-stoichiometric titanium dioxide are very dependent on the extent of the oxygen deficiency in the film. The conductivity mechanism in undoped TiO$_2$ relies on a deficiency of oxygen atoms in the material. These oxygen deficiencies behave like n-type defects, with a typical density of $10^{18} - 10^{19}$ cm^{-3}. As the stoichiometry departs from the ideal Ti:O ratio of 1:2, several changes in the film result. Due to the increased number of oxygen vacancies, the optical absorption in the visible can dramatically increase for these films [19].

I.2.5. Applications of Titanium Dioxide

In recent years, there has been a growing interest in preparing the transparent conducting oxide (TCO) thin films for a wide application in the technological field. Among them, titanium dioxide (TiO_2) is one of the remarkable transparent conducting oxide investigated compounds with many applications in different domain such as: dielectric materials, gas sensors, electro-chromic systems, planar waveguides, antibacterial, antireflection coatings, solar cells and photo-catalysts [5].

I.2.5.1. Application in electrochromic systems

Subjected to an electric field, electrochromic materials have the property of reversibly changing color. These systems therefore make it possible to modulate the transmission of the luminous flux. This property results from the change in oxidation state of the metal cations that make up the oxide. Depending on whether the structure of the thin layer of TiO_2 is amorphous or crystalline, the light transmission will be modulated either by absorption or by reflection. In fact, the structure of electrochromic devices is complex. They are formed by the superposition of three coatings sandwiched between two conductive glass plates. The variation in optical transmission is generally due to the coloring of the electrochromic layer during the insertion of H^+ or Li^+ cations, which corresponds to an oxide of mixed valence depending on the reaction:

$$TiO_2 + xLi^+ + xe^- \leftrightarrow (Li^+)_x TiO_2 \qquad \text{(I.1)}$$
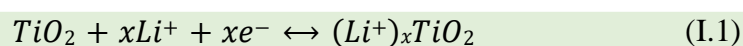
Colorless   blue

Electrochromic materials therefore have a mixed conduction (ionic and electronic). Their properties depend more particularly on the nature of the phase, the degree of crystallinity, the water content. These different parameters are controlled by the conditions of elaboration of the thin layers. Given the advantages of the sol-gel method and the flexibility of its processes, it is suitable for synthesizing this type of material [20].

I.2.5.2. Applications photovoltaic

By converting light energy into electrical energy and taking advantage of the photovoltaic effect that occurs at the junction of a semiconductor, photovoltaic conversion is positioned as a promising alternative to fossil fuels in the global context of the development of renewable energies. The latter does two tasks: it absorbs solar energy and separates electric charges by producing an electron-hole pair. For this to happen, the semiconductor needs to be very pure and free of lattice defects; otherwise, the pair will recombine right away, even before

the electron and hole have a chance to separate. Because of this, creating this kind of material is highly expensive. Michael Grtzel made a significant discovery relating to the usage of TiO_2 in photovoltaics. Only the monolayer of dye molecules in contact with TiO_2 is capable of absorbing light. Barely 1% of the incident light is absorbed on a flat surface. Use a TiO_2 coating made of TiO_2 nanoparticles to improve absorption (Fig.I.4). The roughness of the surface is substantially higher. Thus, while in contact with the electrolyte, more molecules can be adsorbed onto the TiO_2 surface. When exposed to an irradiation energy of 75 mW, the conversion efficiency η is greater than 7% [21].
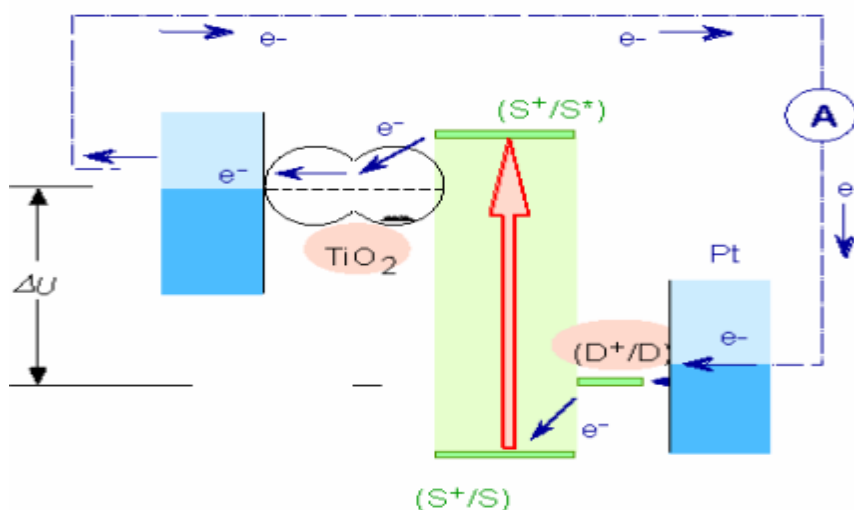
Fig.I.4 Gratzel nanocrystalline photovoltaic cell [21].

I.2.5.3. Gas sensors

At the beginning of the 1960s, there was the discovery of oxide semiconductors which were capable of detecting gases. A component is considered a gas sensor if at least one of its physical characteristics changes when exposed to a change in the gaseous environment.

A sensor typically consists of two basic components: the sensitive element, which is over the reaction with the gas space passes, and the transducer, which is a mechanism that enables the conversion of the reaction's output into a signal that can be easily monitored. The electrical conductivity of a metal oxide changes as it comes into contact with a new gaseous environment, and this variation forms the basis of the detecting mechanism. One of the oxide semiconductors employed is TiO_2, which is particularly useful when doped with impurities because of its improved sensitivity to gases like oxygen gas [8].

I.2.5.4. Photocatalytic applications

The term photocatalyst is a combination of two words: The word photo, which has to do with photons, and a catalyst, which is a chemical that affects the rate of a process when it is present. As a result, photocatalysts are substances that, when exposed to light, alter the rate of a chemical reaction. The term "photocatalysis" refers to the chemical reactions that use light and a semiconductor. In essence, all photocatalysts are semiconductors. A semiconducting substance will produce an electron-hole pair when exposed to light in a process known as photocatalysis.The photocatalysis can be classified into two categories [22]:

❖ Homogeneous photocatalysis: When the semiconductor and reactant are both in the same phase (gas, solid, or liquid).

❖ Heterogeneous photocatalysis: When both the semiconductor and reactant are in different phases.

In semiconductors, the distance between the position of the valence band (VB) and the conduction band (CB) determine the ability of the semiconductor material in the light absorption process and its oxidation-reduction ability (Fig.I.5). In general, the photocatalytic reaction ofTiO_2 includes several basic processes. This process must be thoroughly observed to understand the workings of TiO_2 photocatalysts and is useful for the development of new photocatalysts [22].
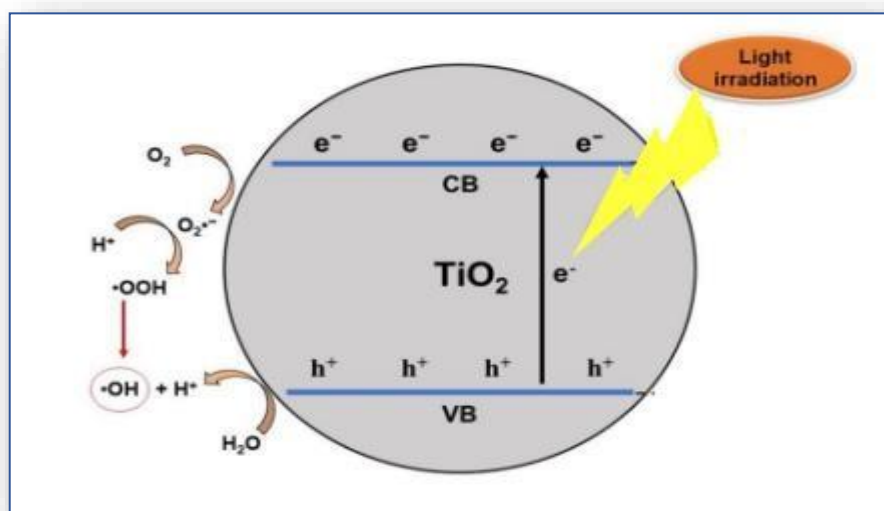
Fig.I.5 Schematic diagram of TiO_2 photocatalytic principle [22].

1. Mechanism of photocatalytic activity

Since it is an appealing method for the total elimination of unwelcome contaminants (pollutants) in both the liquid and gaseous phase by employing solar or artificial light irradiation, TiO_2 heterogeneous photocatalysis has been the focus of numerous studies in recent years [23]. The photocatalytic process is schematized for the case of TiO_2 in the (Fig.I.6), whose main actions are as follows:

A. Excitation of TiO₂

The primary photochemical act, subsequent to near-UV light (wavelengths <400 nm) absorbed by TiO_2 particles, is the generation of electron–hole pairs where the separation (I.1) intoconduction band electrons (e_{CB}^-) and valence band holes (h_{BV}^+) [24]:

$$TiO_2 + hv \longrightarrow TiO_2 + (e^- + h^+) \qquad (I.2)$$
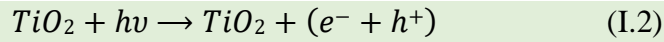
B. Oxidation of water and hydroxides

The second step is linked to the formation of the hydroxyl radical $OH^\bullet$. Indeed, an electron from the valence band is transferred to the conduction band with the formation of a positive hole (h^+). The holes react with electron donors such as H_2O and hydroxide ions (OH^-), resulting from the ionization of water, to form the hydroxyl radical $OH^\bullet$ according to the reactions (I.2) and (I.3) [12]:

$$hv_{UV} + H_2O \longrightarrow OH^- + H^+ \qquad (I.3)$$
$$h^+ + OH^- \longrightarrow OH^\bullet \qquad (I.4)$$
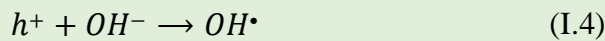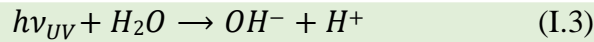
C. Reduction of oxygen

The step occurring simultaneously with the previous one concerns the formation of the hydroperoxyl radical $HO_2^\bullet$. This is due to electrons reacting with dissolved oxygen O_2 to form superoxide radicals $O_2^{-\bullet}$ and protonation of the latter gives rise to the hydroperoxyl radical $HO_2^\bullet$. This step is schematized by the reactions below [12]:

$$e^- + O_2 \longrightarrow O_2^{-\bullet} \qquad (I.5)$$
$$O_2^{-\bullet} + H^+ \longrightarrow HO_2^\bullet \qquad (I.6)$$
$$2\,HO_2^\bullet \longrightarrow H_2O_2 + O_2 \qquad (I.7)$$
$$H_2O_2 + hu_{uv} \longrightarrow 2OH^\bullet \qquad (I.8)$$
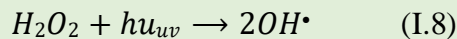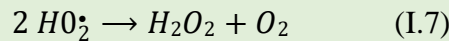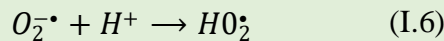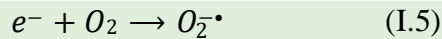
D. Degradation of pollutants

The phenomena of pollutant degradation are the last stage of this photo-catalysis mechanism. As shown by reaction (I.8), the produced hydroxyl radicals also take part

in pollutant degradation [12]:

$$OH^\bullet + Pollutant \rightarrow CO_2 + H_2O \qquad (I.9)$$
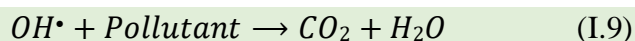
2. Recombination of electron-hole pairs

We must also consider the electron-hole recombination reaction in the volume of the particle or on the surface:

$$h^+ + e^- \rightarrow Heat \qquad (I.10)$$
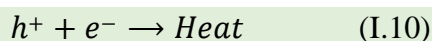
The rate of formation of electron-hole pairs under the impact of photons depends on the intensity of the incident light and the optical and physical properties of the photocatalyst [25].

3. Influence of impurities in the TiO₂ film on the photocatalytic activity

Impurities in the TiO_2 layer can play a beneficial role in photocatalytic activity, when their concentration is controlled. The effect of impurity insertion into the TiO_2 layer was studied by Park et al. The authors tested the photocatalytic activity of thin layers of TiO₂ produced by the sol-gel technique and doped with low valence cations, Fe^{+3}, Co^{+2}, Ni^{+2} and high, Mo^{+5}, Nb^{+5}. The photocatalytic activity of TiO_2 for the conversion of trichlorethylene vapors is significantly higher when the catalyst is doped with Mo, Nb and W rather than with Fe, Co and Ni. This difference may come from the high crystallinity of the samples doped with the high valence cations [26]. Le et al reported that incorporation of donor and acceptor species directly affects electronic structure and in turn, reactivity of photocatalyst. The doping reduces the band gap of photocatalyst, i.e. dispersion of the CB and VB of photocatalysts shows a positive effect after doping. The addition of dopants in photocatalyst exhibits enhanced performance because it avoids electron-hole recombination and extends sensitivity towards a broad range of spectrum [27].

4. Degradation of dye pollutants

The removal of non-biodegradable organic dyes and other chemicals from the environment is a central ecological problem. Dye molecules are not degraded easily due to the complex aromatic structure and xenobiotic properties. Thus, it is necessary to develop different effective treatment methods and techniques for the removal of these toxic dye contaminants. Recently semiconductor photocatalysts also termed as heterogeneous photocatalysts have been used as a promising method for the removal of carcinogenic contaminants from industrial effluents since they not only degrade but also cause complete mineralization of pollutants to

H_2O, CO_2 and mineral acids. Different semiconductor metal oxides have been used, including TiO_2, ZnO, Fe_2O_3, PbO_2, SnO_2, Sb_2O_5, etc [17].

5.Advantages of photocatalysis

Photocatalysis has several advantages among which we can mention [28]:

✓ Good dye destroying technique.

✓ Total mineralization possible: formation of H_2O and CO_2 and other species.

✓ It operates at ambient temperature and pressure.

✓ Catalyst used non-toxic, active in different physical forms, inexpensive.

✓ It requires low energy consumption.

I.2.6. Kinds of doped semiconductors

Semiconductor doping simply means the purposeful introduction of impurities or dopant into an extremely pure semiconductor. This is because as the band gap of a material increases it becomes difficult to dope them in regular (p and n type) semiconductors [29], (see Fig.I.6).

➢ **n type semiconductor**

An intrinsic semiconductor with added donor-type impurities is a typical semiconductor (n). Because they have an excess of electrons, the materials that result from this process are known as n-type semiconductors. A pseudo-energy level immediately below the conduction band appears as a result of the addition of electron-donor atoms. As a result, compared to an inherent semiconductor, the energy required for the electrons to transit through the conduction band is significantly easier to get [13].

➢ **p type semiconductor**

These are semiconductors in which acceptor impurities have been voluntarily added. Similar to how valence electrons must be supplied with energy to pass on this acceptor level, the introduction of electron-acceptor atoms results in the emergence of a level above the band, and the electrons' departure causes the creation of holes in the valence band [13].
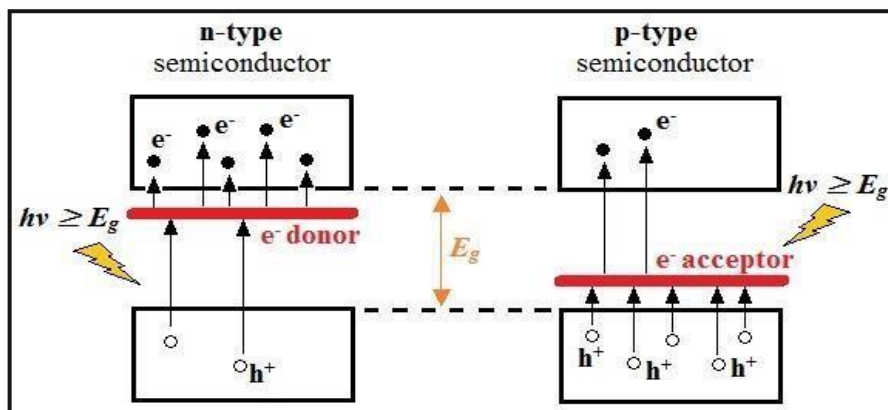
Fig.I.6 Illustration of n and p type semiconductor [30].

I.2.6.1. Elements doped Titanium dioxide

Titanium dioxide TiO_2 can be used pure or doped with metals or metal oxides. It has been shown in some cases that doping gives rise to an increase in its photoactivity and improves its electrical and magnetic properties. The determining parameters that can influence the properties of the doped materials are: the method of synthesis, the concentration, the nature of the dopant and the heat treatment [31].

➢ **Cation doping with transition metals**

The doping of TiO_2 dioxide with transition metals is one of the most important approaches and several works have been carried out with different metals: iron (III), zirconium, cerium, manganese, chromium and cobalt, tungsten, silver.

Several authors report that this type of cationic doping decreases the energy threshold of TiO_2 by reducing the width of its forbidden band. However, the majority of works adhere to the fact that these doping increases the recombination of charges [21].

➢ **Anion doping with non-metals**

It was at the beginning of the 1990s that the first report on anionic doping was carried out by Sato et al., using nitrogen, evaluated on the basis of calculations of densities of states, the effect of all the non-metallic dopants already mentioned. They concluded from these calculations that nitrogen doping is the most effective among all other non-metallic dopants [21].

I.2.6.2. Choice of Cesium as a doping element

TiO$_2$ is one of the most studied semiconductor materials, as is evident from more than 50000 papers published over the past 40 years on this material (with a still strongly increasing publication rate over the past decade) [32]. Many studies had been attributed to the doping of transition metals into TiO$_2$ thin films such as Nb, Al, Fe, Ga. Studies on doping processes are not limited to these, but there are also studies reported by various researchers using different elements. Doping transition metal is one of the most effective and simplest routes to improve the properties of TiO$_2$ thin films, because the transition metals can modify the energy band gap and introduce charge traps for photo-generated carrier. The research about Cesium doping TiO$_2$ thin films is considered few. For harvesting optoelectronic properties of (TiO$_2$: Cs), we have chosen Cs as dopants for two reasons: (1) As the ionic radii of Cs$^+$ is 0.165 nm comparing to that of Ti^{+4} (0.061 nm), (2) its availability and nontoxicity. Cs element has +1 valence state, therefore, they can provide three extra electrons when bonded with the divalent TiO_2 structure.

References

[1] **S. Andreas**, Transparent conducting oxides—an up-to-date overview, Mater (5) (2012), pp 661-683.

[2] **K. Chopra, L. Major, D. K. Pandya**, Transparent conductors—a status review, Thin solid films, 102(1) (1983), pp 1-46.

[3] **A. Abdlekrim**, « Optimisation des conditions d'élaboration des couches minces d'oxyde d'étain SnO$_2$ par spray », thèse de doctorat, université de Biskra, (2016).

[4] **C. Khelifi**, « Tin dioxide SnO$_2$ thin films deposited by ultrasonic spray technique: Properties and Applications», doctoral dissertation, university of Biskra, (2018).

[5] **A. Attaf, A. Derbali, H. Saidi, A. Bouhdjer, M. S. Aida, R. Messemeche**, Precursor concentration effect on the physical properties of transparent titania (Anatase-TiO$_2$) thin films grown by ultrasonic spray process for optoelectronics application, Optical Materials, 132(2022), pp 112790.

[6] **Bouabellou, Y. Bouachiba**, « Synthèse de films TiO$_2$ et étude structurale et optique », mémoire de magister, Université de Constantine, (2017).

[7] **I. Sta, M. Jlassi, M. Hajji, M. F. Boujmil, M. Kandyla, H. Ezzaouia**, Structural and optical properties of TiO$_2$ thin films prepared by spin coating, Journal of sol-gel science and technology, 72(2014), pp 421-427.

[8] **S. Chala**, « L'effet de dopage par l'aluminium sur les propriétés des couches minces du TiO$_2$ élaborées par voie Sol-Gel (spin caoting) », mémoire de master, université de Biskra, (2017).

[9] **R. Messemeche, H. Saidi, A. Attaf, Y. Benkhetta, S. Chala, R. Azizi, R. Nouadji**, Elaboration and characterization of nano-crystalline layers of transparent titanium dioxide (Anatase-TiO$_2$) deposited by a sol-gel (spin coating) process, Surfaces and Interfaces, 19(2020), pp 100482.

[10] **L. Li, C. Liu, and Y. Liu**, Study on activities of vanadium (IV/V) doped 2 (R) nanorods induced by UV and visible light, Materials Chemistry and Physics, 113(2-3) (2009), pp 551-557.

[11] **M. C. Benachour**, « Elaboration et caractérisation des couches minces de TiO$_2$ dopées à l'erbium, à différentes températures et épaisseurs », mémoire de magister, université de Constantine, (2017).

[12] **S. Abbad**, « Etude de l'effet du dopage et des parametres de synthese de poudres nanocristallines de TiO₂ preparees par sol-gel sur les proprietes physiques et photo-catalytiques », doctoral dissertation, Université d'Oum El Bouaghi, (2022).

[13] **H. Meddas**, « Effet du dopage par l'azote sur les propriétés des films minces de dioxyde de titane préparés par procédé sol gel (spin coating) », université de Biskra, (2020).

[14] **T. Goudjil**, « Etude de l'oxyde de titane en couches minces en hétérojonction avec le silicium, application photovoltaïque », doctoral dissertation, Université Mouloud Mammeri, (2013).

[15] **I. Ali, M. Suhail, Z. A. Alothman**, Recent advances in syntheses, properties and applications of TiO₂ nanostructures, RSC advances, 8(53) (2018), pp 30125-30147.

[16] **N. GUERFI**, « Synthèse, caractérisation et propriétés photocatalytiques de couches minces de TiO2 », mémoire de master, université de Biskra, (2021).

[17] **R. messemche**, « Elaboration and characterization of undoped and doped titanium dioxide thin layers by sol gel (spin coating) for photocatalytic applications », doctoral dissertation, université de biskra, (2021).

[18] **T. Beuvier**, « Des nanotitanates de sodium aux dioxydes de titane : électrode négative à base de TiO₂ (B) nanométrique pour accumulateur lithium-ion », doctoral dissertation, université de Nantes, (2009).

[19] **B. S. Richards**, « Novel uses of titanium dioxide for silicon solar cells », doctoral dissertation, UNSW Sydney, (2002).

[20] **F. Medjaldi, A. Bouabellou**, « Préparation et caractérisation de couches minces d'oxyde de titane (TiO₂) et du couple d'oxydes (TiO₂/SnO₂) », mémoire de magister, université de Constantine, (2017).

[21] **B. O'regan, M. Grätzel**, A low-cost, high-efficiency solar cell based on dye-sensitized colloidal TiO2 films, Nature, 353(6346) (1991), pp 737-740.

[22] **D. R. Eddy, M. D. Permana, L. K. Sakti, G. A. N. Sheha, I. Rahayu**, Heterophase polymorph of TiO₂ (Anatase, Rutile, Brookite, TiO₂ (B)) for efficient photocatalyst: fabrication and activity, Nanomaterials, 13(4) (2023), pp 704.

[23] **I. M. Arabatzis, T. Stergiopoulos, M. C. Bernard, D. Labou, S. G. Neophytides**, Silver-modified titanium dioxide thin films for efficient photodegradation of methyl orange. Applied Catalysis B: Environmental, Applied Catalysis B: Environmental, 42(2) (2003), pp 187-201.

[24] **J. I. Kroschwitz, M. Howe-Grant, R. E. Kirk, D. F. Othmer**, Encyclopedia of chemical technology. John Wiley & Sons (1996).

[25] **A. Boumezoued, K. Guergouri**, « Etude et préparation par Sol-Gel de nanomatériaux à base d'oxydes semiconducteurs et leurs applications », doctoral dissertation, (2020).

[26] **C. Sarantopoulos**, « Photocatalyseurs à base de TiO_2 préparés par infiltration chimique en phase vapeur (CVI) sur supports microfibreux », doctoral dissertation, université de Oum El Bouaghi, (2007).

[27] **R. Ameta, M. S. Solanki, S. Benjamin, S. C. Ameta**, Photocatalysis. In Advanced oxidation processes for waste water treatment, Academic Press, (2018), pp. 135-175.

[28] **A. Bazine, M. S. Ferah**, « Elaboration par sol-gel et caracterisation d'oxyde metallique (type : α-fe2o3) aux propries photocatalytiques », doctoral dissertation, université Frères Mentouri-Constantine 1, (2017).

[29] **S. M. Al-Shomar,** Investigation the effect of doping concentration in Ruthenium-doped TiO2 thin films for solar cells and sensors applications, Materials Research Express, 7(3) (2020), pp 036409.

[30] **O. Monfort, G. Plesch**, Bismuth vanadate-based semiconductor photocatalysts: a short critical review on the efficiency and the mechanism of photodegradation of organic pollutants, Environmental Science and Pollution Research, 25(20), pp 19362-19379.

[31] **H. Dehdouh, R. Bensaha**, « Propriétés physico-chimiques des couches minces de l'oxyde de titane. Effet de la concentration », mémoire de magister, université de Constantine, (2017).

[32] **Y. C. Nah, I. Paramasivam, P. Schmuki**, Doped TiO_2 and TiO_2 nanotubes: synthesis and applications, ChemPhysChem, 11(13) (2010), pp 2698-2713.

Chapter II

Sol-gel (spin-coating) and characterization methods

This chapter has been divided into three parts. The first part is devoted to the definition and mechanism of thin films formation. In the second part, a description was given of the various techniques for depositing thin layers and in particular the Sol gel process. In the last part, we presented the principle of the deferential methods used to characterize thin layers.

II.1. General concept of thin films

II.1.1. Definition

In principle, a thin layer of a given material is the material deposited on a support called a substrate, one of the dimensions (thickness) of this deposit has been greatly reduced so that it is expressed in nanometers [1]. This small distance between the two boundary surfaces of the material leads to a disturbance of the physical properties along this dimension [2].

II.1.2. Difference between bulk state and thin film of the material

The essential difference between the material in the bulk state and that in thin layers is that in the bulk state one generally neglects with good reason in the role of the limits in the properties, while in a thin layer they are, on the contrary, the effects related to boundary surfaces which are preponderant. It is quite obvious that the lower the thickness, the greater this two-dimensional effect. However, when the thickness exceeds a certain threshold, its effect will become minimal and the material will regain the well-known properties of solid material [3].

II.1.3. Relation between thin layer and substrate

The second essential characteristic of a thin layer is whatever the procedure used for its manufacture, a thin layer is always attached to a substrate on which it is built. Consequently, it will be imperative to take into account this major fact in the design, namely that the support has a very strong influence on the structural properties of the layer. Thus, a thin layer of the same material of the same thickness may have substantially different physical properties depending on whether it is deposited on an amorphous insulating substrate such as glass, or a monocrystalline silicon substrate for example [4].

II.1.4. Thin film modes and growth mechanisms

All processes for the production of thin films are carried out in three stages:

a) The production of appropriate ionic, molecular, atomic species

b) The transport of these species to the substrate

c) Condensation on this same substrate is done either directly or by through a chemical or electrochemical reaction to form the solid deposit. This step often goes through three phases:

nucleation, coalescence then growth [1].

Nucleation

The islands formed develop by collisions with atoms on the surface of the substrate. Upon reaching their critical size corresponding to a maximum free energy, the islands absorb other atoms and the subcritical islands, it is nucleation.

Coalescence

A first stage of coalescence corresponds to the growth of stable islands by absorption of the smallest by the largest. This stage differs from a second, faster stage of large-scale coalescence where the islands, having reached a critical density, flatten out to increase their surface area and join together. If the probability that all the islands on the substrate are of the same orientation is low, the coalescence produces a polycrystalline deposit, otherwise a thin monocrystalline layer develops [3].

Growth

Once the coalescence of the islands is complete, the addition of material allows the layers to develop in thickness after a slow filling of the empty channels. The growth can be two-dimensional or three-dimensional depending on the relative values of the interaction energies atom-atom of the film and atom of the film-atom of the substrate. In a simple approach, we classify the growth of thin films on a substrate into three categories [5] (see Fig.II.1):

a) The island type (called Volmer-Weber).
b) The diaper type (called Frank-van der Merwe).
c) The mixed type (called Stranski-Krastanov).
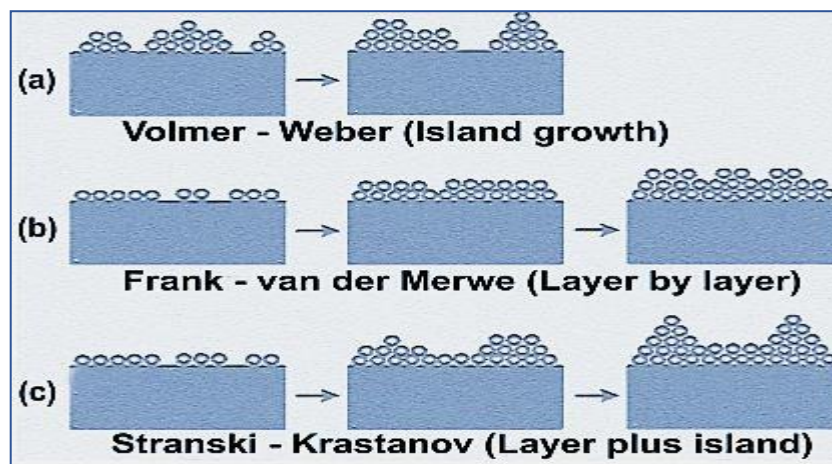
Fig.II.1 Thin film growth modes [6].

II.1.5. Thin film deposition procedure

All thin film deposition processes contain four successive steps, as shown in Fig.II.2. The source which constitutes the basic material of the thin film to be produced can be a solid, a liquid, a vapor or a gas. When the material is solid, its transport to the substrate takes place by vaporization. This can be achieved by thermal evaporation, electron gun, laser ablation or positive ion 'sputtering'. All of these methods are classified under the name of physical vapor deposition PVD. The solid source is occasionally transformed into vapor by chemical means. In other cases, the base material is in the form of a gas or a liquid have the sufficient vapor pressure to be transported at moderate temperatures. Processes that use gases, evaporated liquids or chemically evaporated solids as a base material are known as chemical vapor deposition (CVD) "Chemical vapor deposition" [5].
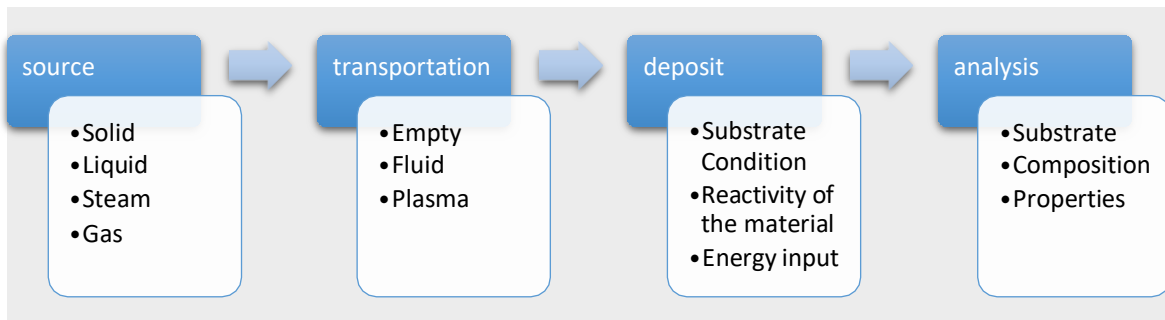
Fig.II.2 Diagram of the steps of the thin film manufacturing process [5].

II.1.6. Application of thin films

In today's society, thin films are used in a wide range of products, including mirrors, cutting tools, eyeglasses, microelectronics, window glass, and solar cells. It is very significant and important for a wide range of industrial applications and can satisfy a very broad range of needs for certain industrial or scientific applications. Although thin film technology has made incredible strides. Wear, corrosion, and resistant coatings are a few of the crucial applications; nevertheless, the choice of a specific method for the deposition of thin films can be based on a number of factors. Thin films are typically utilized when it is necessary to improve or alter the surface qualities of an object (substrate) by adding to or altering its usefulness [7].

II.1.7. Thin films depositions techniques

Thin layers can be made using a wide variety of techniques due to the diversity of applications for this material. These techniques are generally classified into two broad categories: chemical methods and physical methods. Fig.II.3 below mentions some of them:

```
┌─────────────────────────────────┬─────────────────────────────────────┐
│  Physical deposition            │  Chemical deposition                  │
│                                 │                                       │
│    ┌─────────────────────┐      │     ┌───────────────────────┐         │
│    │ Evaporation         │      │     │ Sol-gel technique     │         │
│    │ techniques          │      │     └───────────────────────┘         │
│    └─────────────────────┘      │     ┌───────────────────────┐         │
│    ┌─────────────────────┐      │     │ Chemical bath         │         │
│    │ Sputtering          │      │     │ deposition            │         │
│    │ techniques          │      │     └───────────────────────┘         │
│    └─────────────────────┘      │     ┌───────────────────────┐         │
│                                 │     │ Spray pyrolysis       │         │
│                                 │     │ technique             │         │
│                                 │     └───────────────────────┘         │
│                                 │     ┌───────────────────────┐         │
│                                 │     │ Plating               │         │
│                                 │     └───────────────────────┘         │
│                                 │     ┌───────────────────────┐         │
│                                 │     │ Chemical vapor        │         │
│                                 │     │ deposition (CVD)      │         │
│                                 │     └───────────────────────┘         │
└─────────────────────────────────┴─────────────────────────────────────┘
```
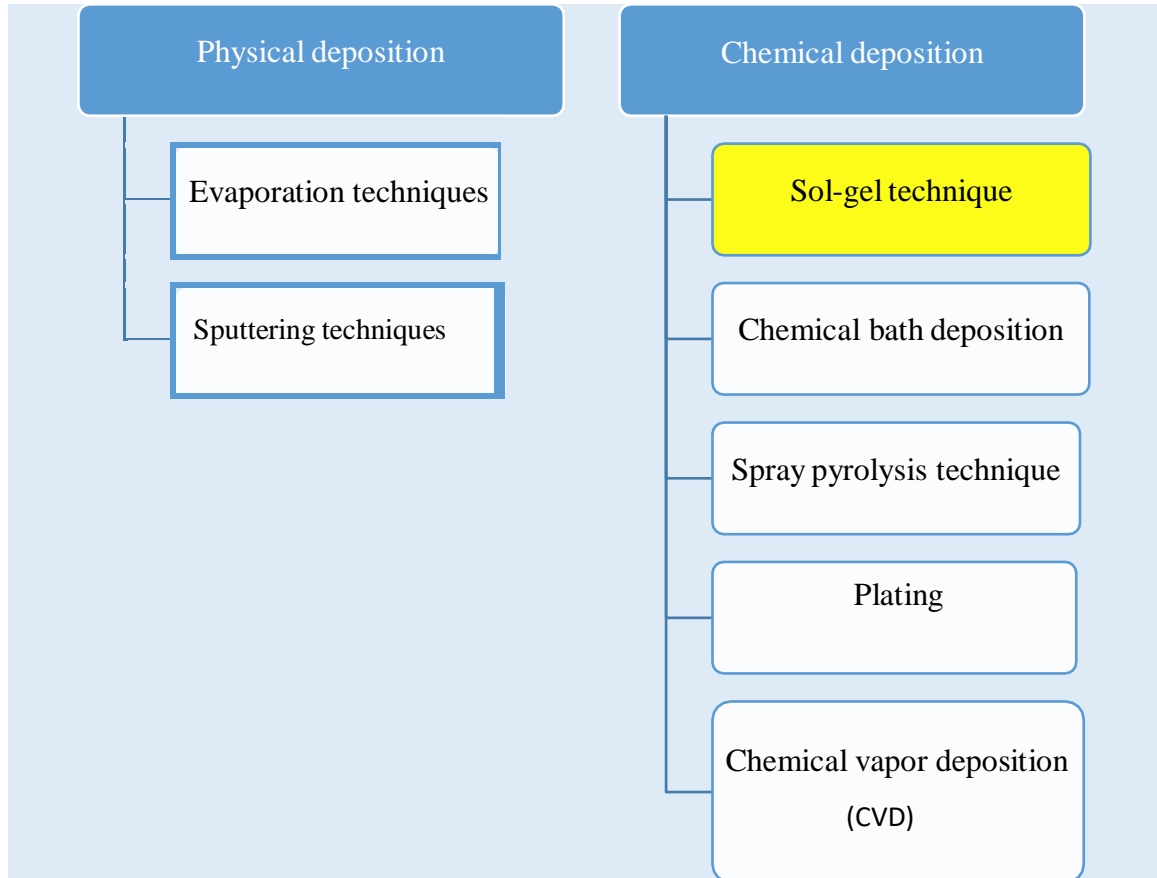
Fig.II.3 Different methods of thin films deposition techniques [8].

II.2. Sol gel technique

In this part, we will describe the basic principle which was used in the development of our samples namely "Sol-Gel" route of thin layers of doped titanium oxide, followed by an exhaustive reminder of the technique of spin coating deposit thanks to which we were able to deposit our thin layers.

II.2.1. Definition

Before going into the details of the sol gel process, it is necessary to recall a few definitions:

Sol: A "Sol" state can be defined as a stable dispersion of species within a solvent.

A dispersion of colloidal particles or molecular entities of a size which must be small enough so that the forces responsible for the dispersion (Brownian motion, Van der Waals interaction) are not overcome by gravity. The aggregation or polymerization of these precursors leads to the formation of an interconnected and stable three-dimensional network, called gel.

Gel: A gel is defined as a two-phase system in which the solvent molecules (water: aquagel or hydrogel, alcohol: alcogel) are trapped in the solid network. The "gel" phase is therefore a solid, amorphous, three-dimensional interconnected network, included in a liquid phase (swollen by a solvent) in a stable manner and containing sub-micrometric pores [9].

II.2.2. Basic idea of the sol-gel process

The basic idea of the sol-gel process, which is the abbreviation of Solution-Gelification, consists in hydrolysing a precursor of the solution using the humidity of the air, in order to obtain a sol (suspension of small macromolecules of a size less than 10 nm). The gel (elastoplastic amorphous solid, formed by a three-dimensional reticulated network) is obtained by polymerization of the sol. A thermal drying pretreatment at a temperature close to 100°C, followed by thermal annealing at an appropriate temperature, makes it possible to densify this gel, thus leading to a solid material [10].

II.2.3. Precursors

A precursor is a chemical reagent which makes it possible to initiate the reaction: it is often an alkoxide (alkoxide of formula $M(OR)_n$: where M is a metal, for example Zn, Al…, and R an organic alkyl group C_nH_{n-1}) or else a metallic salt. Sol-gel synthesis routes [1]:

Inorganic or colloidal route
- obtained from metallic salts (chlorides, nitrates, oxychlorides) in aqueous solution. This route is inexpensive but difficult to control, which is why it is still very little used. However, it is the preferred way to obtain ceramic materials.

Metallo-organic or polymeric route
- obtained from metal alkoxides in organic solutions. This route is relatively expensive but allows fairly easy control of the particle size.

Fig.II.4 The precursors of sol

II.2.4. Reaction mechanisms

The detail of the different stages of formation of the oxide will then make it possible to understand the role of each constituent of the solutions developed. The sol-gel process is based on two reactions: hydrolysis and condensation.

II.2.4.1. Hydrolysis

In order for the alkoxides to condense at room temperature, the hydrolysis of the –OR groups must trigger the reaction process. This step is necessary to give rise to hydroxyl groups –OH:

$$M(OR)_n + H_2O \longrightarrow HO - M(OR)_{n-1} + ROH \qquad \text{(II.1)}$$
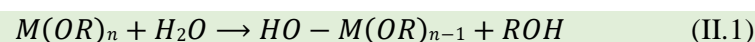
▪ Hydrolysis is a nucleophilic substitution of an –OH ligand for an –OR ligand. It is accompanied by the consumption of water and the release of alcohol. During this step, the functionality of the precursor is created with respect to what is called polycondensation [11].

II.2.4.2. Polymerization

Polymerization often begins before hydrolysis is completely complete. The phenomenon is complex because four mechanisms (alcoxolation, oxolation, alcoholation, and olation) can compete for polymerization. The relative importance of each of the mechanisms depends on the experimental conditions.

A. Polycondensation

First of all, the hydroxyl group formed during hydrolysis is much better nucleophilic than the alkoxide group. It follows that the hydroxyl group reacts by nucleophilic substitution with a mechanism analogous to hydrolysis. It will form a M-O-M bridge with a temporary increase in the coordination of the metal. Two mechanisms then enter into competition: alcoxolation and oxolation.

i. Alcoxolation

This reaction occurs between two metal alkoxides, only one of which has been partially hydrolyzed:

$$(RO)_{n-x}M(OH)_x + M(OR)_n \longrightarrow (RO)_{n-x}(OH)_{x-1}M - O - M(OR)_{n-1} + ROH \qquad \text{(II.2)}$$
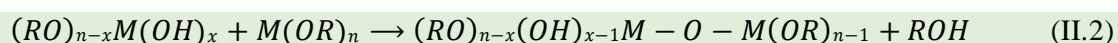
Its reaction mechanism is similar to that of hydrolysis.

ii. Oxolation

This mechanism occurs between two partially hydrolyzed alkoxides:

$$(RO)_{n-x}M(OH)_x + (RO)_{n-y}M(OH)_y \longrightarrow (RO)_{n-x}(OH)_{x-1}M - O - M(OH)_{y-1}(RO)_{n-y} + H_2O$$

(II.3)
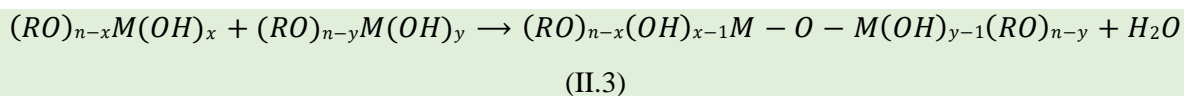
The mechanism remains the same except that the leaving group is a water molecule. Like hydrolysis, polycondensation reactions do not increase the coordination of metal centers [12].

B. Coordination polymerization

These mechanisms take place when the coordination of the metal is not satisfied in its alkoxide form (N-Z $\neq$ 0), where N is the maximum coordination number of the metal cation and Z the degree of oxidation of the metal in the alkoxide. In this case and provided that the steric hindrance due to the ligands allows it, an M-OX-M bridge can be formed. There too, two mechanisms compete: alcoholation and olation. It is a simple nucleophilic addition between a negatively charged OR (alcoholation) or OH (olation) group and a positively charged metal center.

i. Alcohol

It does not need hydrolysis to set up:

$$2M(RO)_nM - OR - M(RO)_{n-1} \qquad \text{(II.4)}$$
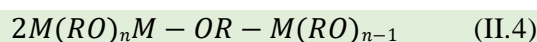
It is the alcoholation that induces the molecular complexity of the species during the polymerization by forming oligomers before adding water. Before the hydrolysis step begins, it is generally difficult to form molecules with large masses, this reaction being highly sensitive to the steric hindrance of the system.

ii. Olation

It requires a hydrolysis of the prior alkoxide of a metal alkoxide:

$$M(RO)_n(HO)_xM(RO)_{n-x} \longrightarrow (RO)_nM - OH - M(OR)_{n-x}(OH)_{x-1} \qquad \text{(II.5)}$$
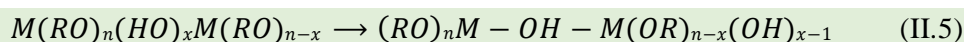
The relative importance of each contributor's contributions greatly influences the structure and morphology of the oxide that results from these reactions. These contributions can be improved by changing the experimental parameters that are related to the network's internal (the nature of the metal atom and alkyl groups, the structure of the molecular precursors, and the reactivities of the alkoxides) and external (the rate of hydrolysis and complexation, the catalyst's properties, the concentration of the metal alkoxide, the solvent, and

the temperature) parameters [13].

II.2.5. Parameters influencing reaction kinetics

The most important influences are mentioned in Fig.II.5 [14]:

Temperature	• It has an influence on the hydrolysis and condensation rates as soon as the soil is prepared, then during aging or storage. Obviously, the higher it is, the faster the reactions.
Influence of pH	• An acidic pH accelerates hydrolysis and slows down condensation unlike a basic pH. A high rate of hydrolysis (acid pH) therefore promotes the growth of the network and leads to a polymer solution.
The choice of alkoxide and its concentration	• This choice is made according to the reactivity of the alkoxide, and the type of sample that one wants to develop. As for the concentration in the ground, it is especially important during condensation; in fact, the weaker it is, the further apart the molecules capable of binding are, which delays the reactions.

Fig.II.5 Parameters influencing reaction kinetics.

II.2.6. Advantages of sol gel technique

There are other methods for creating thin films, but the sol-gel technique offers the best chances for producing homogenous, large-area oxide films at cheap cost, low crystallization temperature, and high vacuum-free conditions [15]. It provides low energy costs, high purity and superior homogeneity of the material, realization of multi-component deposits in a single operation, and simplicity of equipment and ease of material implementation [16]. Additionally, using this strategy makes it simpler to incorporate dopants. Therefore, this method is appropriate for cutting-edge research [17].

II.2.7. Densification of thin layers

The gel deposition and formation step is followed by two other operations: drying and annealing. Drying was done to remove almost all of the solvent. After drying, the gel undergoes an annealing heat treatment intended to transform it into a dense ceramic film.
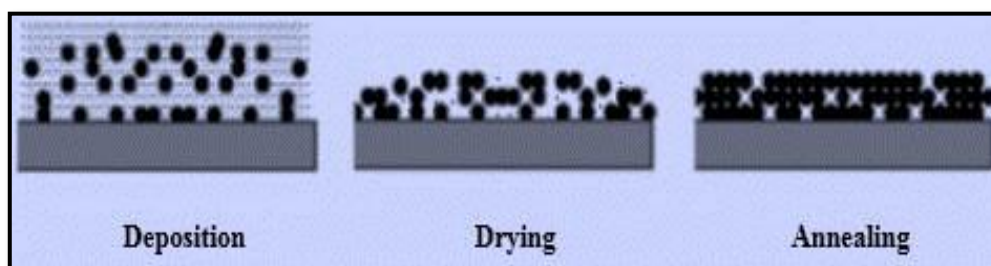
a. Drying thin layers

The drying of the deposited layer is a very important step in the production of quality materials; it corresponds to the evaporation of residual solvents by diffusion through the pores [15].

b. Annealing of thin layers

The heat treatment or annealing, allows on the one hand the elimination of the residual organic species after drying, and on the other hand the densification of the material by crystallization. It is only after annealing that the desired material can be obtained. Indeed, after drying, the organic groups of Alkyl type (-OR-) are still present in the deposited film. Only annealing can eliminate them (Fig.II.6). Annealing's are generally carried out at temperatures between 300°C and 1400°C depending on the type of substrate [14].

Fig.II.6 Influence of drying and annealing on the porosity of thin layers [15].

II.2.8. Different sol gel processes

The two best-known processes for producing thin layers with control of the deposited thickness are dipping-shrinking (dip coating) and spin-coating (spin coating). Both are used at ambient temperature and pressure. The thicknesses of the films are controlled by varying the deposition rate [1].

II.2.8.1. Dip coating process

Dip coating designates the deposition of a wet liquid film by withdrawal of a substrate from a liquid coating medium. The process of film formation in total implies several technical stages as demonstrated in Fig.II.7, but nevertheless the underlying chemical and physical processes are mostly overlapping. Starting with the immersion of the substrate, a coherent liquid film is entrained on the withdrawal of the substrate from the coating fluid, which then consolidates by drying and accompanying chemical reactions. To obtain the final coating material, normally a further curing or sintering step (post-treatment) is then necessary [16].
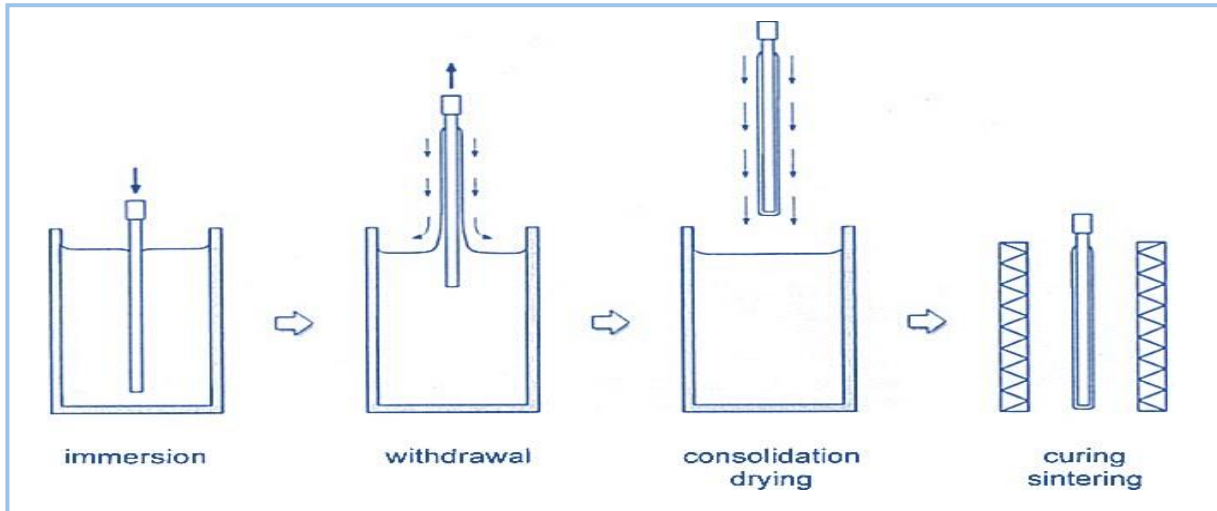
Fig.II.7 Fundamental stages of sol-gel dip coating [16].

II.2.8.2. Spin Coating process

a. Definition

Spin coating is a batch procedure in which a liquid layer is applied on a revolving substrate using centrifugal force [16]. In a typical procedure, a small puddle of fluid resin is applied to the middle of a substrate, and the substrate is then spun rapidly (usually at a speed of roughly 3000 rpm). A thin resin film will form on the surface as a result of the resin spreading to and eventually departing the substrate's edge due to centrifugal force. The type of resin (viscosity, drying rate, percent solids, surface tension, etc.) and the spin process parameters that are selected will determine the final film thickness and other attributes. The qualities of coated films are characterized in terms of final rotational speed, acceleration, and fume exhaust [17].

b. Key stages of spin coating

Bornside, Macosko, and Scriven (1987) and Scriven (1988) offer a fantastic explanation of the spin-coating procedure. They outline the deposition, spin-up, spin-off, and evaporation phases of spin coating (Fig.II.8). The substrate is often raised to its final rotation rate in a fraction of a second. Deposition and spin-up happen swiftly. Concurrently, spin-off and evaporation take place [18].
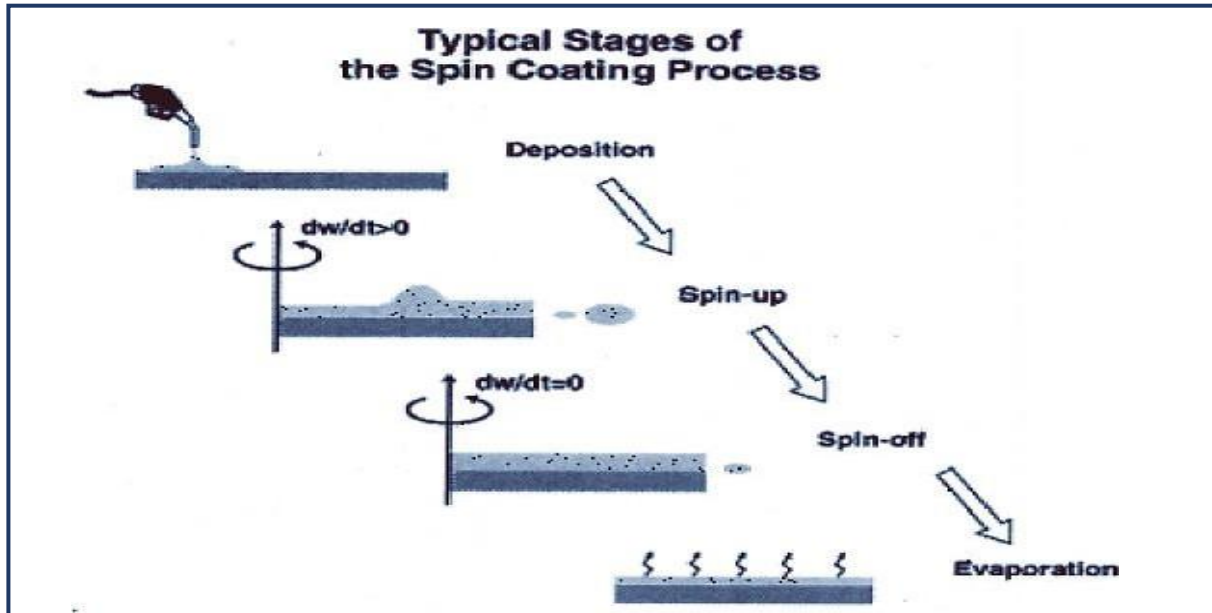
Fig.II.8 Key stages of spin coating process [19].

1. Deposition

At this stage, the substrate is accelerated to the necessary speed while the solution is allowed to fall onto rotating substrates from micro syringes. Due to centrifugal force, the solution spreads and its height is lowered to a critical level. At this stage, a piece of the substrate's surface is quickly covered or "wetted" with an excess of the liquid to be coated. The amount of liquid that may be deposited through excessive, regardless of the method, is limited, and this stage terminates when distribution stops.

2. Spin up

The substrate is accelerated in the second step to reach its desired, ultimate rotation speed. During this step, the rotational motion of the wafer typically causes forceful fluid expulsion from the wafer surface. Spiral vortices may temporarily exist during this stage due to the initial depth of fluid on the wafer surface; these would develop as a result of the twisting motion brought on by the inertia that the top of the fluid layer exerts while the wafer below rotates faster and faster. Eventually, the fluid becomes so thin as to rotate entirely with the wafer, erasing all traces of fluid thickness variations. When the fluid is thin enough and the wafer has reached its ideal speed, the viscous shear drag precisely balances the rotating accelerations [19].

3. Spin off

In the third stage, fluid viscous forces predominate over fluid thinning behavior while

the substrate is spinning continuously. The fluid gradually thins during this period. Although fluid thinning is often relatively uniform, interference colors can sometimes be seen "spinning off" in solutions containing volatile solvents, and they do so gradually more slowly as the coating thickness is decreased.

4. Evaporation

The film drying stage starts after the spin-off step is finished. Centrifugal outflow ends at this point, and solvent loss causes additional shrinking. On the substrate, a thin layer is created as a result. The suspended or dissolved solids may become so concentrated at the liquid surface during the evaporation stage that they create a solid skin with a high viscosity and low diffusivity [19].

II.2.8.3. Advantages and disadvantages of spin coating process

✦ Advantages

Spin coating technology is a desirable technique for thin film deposition for a number of reasons, including its affordability, lack of safety risks, ease of scaling up, growth occurring at a relatively low temperature, and compatibility with flexible organic substrates. Additionally, a number of variables (such as spin speed, spin time, acceleration, fume exhaust, etc.) can be adjusted to successfully control the end products' morphologies and qualities. Spin coating has been shown to be a very effective and adaptable method for producing nanostructures. The spin coating technique's outstanding benefit is its controllability and reproducibility of the coating process, which also offers a firm control over the morphologies and properties of the generated films.

✦ Disadvantages

Despite its many benefits, spin coating has a few drawbacks that are becoming increasingly significant as substrate sizes grow and photoresist prices rise. Large substrates are unable to be spun quickly enough to allow the film to thin. The inefficient use of materials is its main flaw. Only 2-5% of the material poured onto the substrate is typically used in spin coating operations; the other 95–98% is thrown off into the coating bowl and discarded [17].

II.3. Characterization methods

After having produced the thin layers, their structural, microstructural and optical characterization is then carried out. X-ray diffraction (XRD), UV-Vis spectrophotometry, Four-point probe method and Scanning Electron Microscopy are the main analysis techniques used.

II.3.1. X-ray's diffraction (XRD)

X-rays are fired into a sample of crystalline solids in accordance with Bragg's Law, which causes the rays to diffract in all directions. The detector tracks the X-ray beam diffracted by the sample at a constant angular velocity. Lattice planes in crystalline solids or powder samples are randomly organized and may be oriented in numerous ways. The material's characteristic diffraction pattern can be seen in the X-ray diffraction that was obtained [20]. The fundamental idea behind XRD is shown in Fig.II.9.
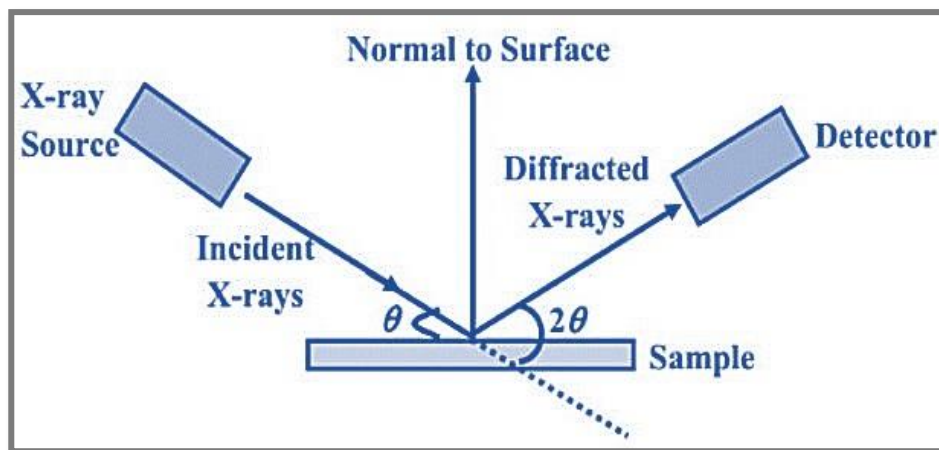
Fig.II.9 Illustration of basic principle of XRD [20].

The incident ray in the figure above has an angle (θ) and a distance (d), which determines the lengths of the various light paths. The Bragg equation can be used to analyze the phenomena that result in constructive wave interference. The Bragg equation follows:

$$2d_{hkl} \sin \theta = n\lambda \qquad (\text{II.6})$$

Where n is the diffraction order (1, 2, 3, and so on), d_{hkl} is the distance between planes of atoms in the crystal (plane with a certain Miller index), θ is the diffraction angle, and λ is the wavelength of the X-rays used (1.5406 Å) [20]. The crystallite size of the elaborated sample is estimated from the full width at half maximum (FWHM) of the most intense diffraction line by Scherrer's formula as follows [21]:

$$D = \frac{0.9\lambda}{\beta \cos \theta} \qquad (\text{II.7})$$

D: The crystallite size (nm or Å).

λ: The wavelength of X-ray (nm or Å).

β: The full width at half maxima of the peak (FWHM) in radians.

θ: Bragg's angle in radians.

It can be calculating the dislocation density using the grains size value according tothe following relationship [21]:

$$\delta = \frac{1}{D^2} \qquad \text{(II.8)}$$

The micro-strain (ꜱ) of the films were calculated using the following equations [22]:

$$\varepsilon = \frac{\beta}{4 \tan \theta} \qquad \text{(II.9)}$$

II.3.2. Spectroscopy (UV-VISIBLE)

UV spectroscopy is a type of absorption spectroscopy in which a molecule absorbs light in the ultra-violet region (200-400 nm). Ultraviolet radiations that are absorbed cause the electrons to be excited from their ground state to a higher energy state. The energy difference between the ground state and higher energy states is equal to the energy of the ultraviolet radiation that is absorbed [23], (see Fig.II.10).
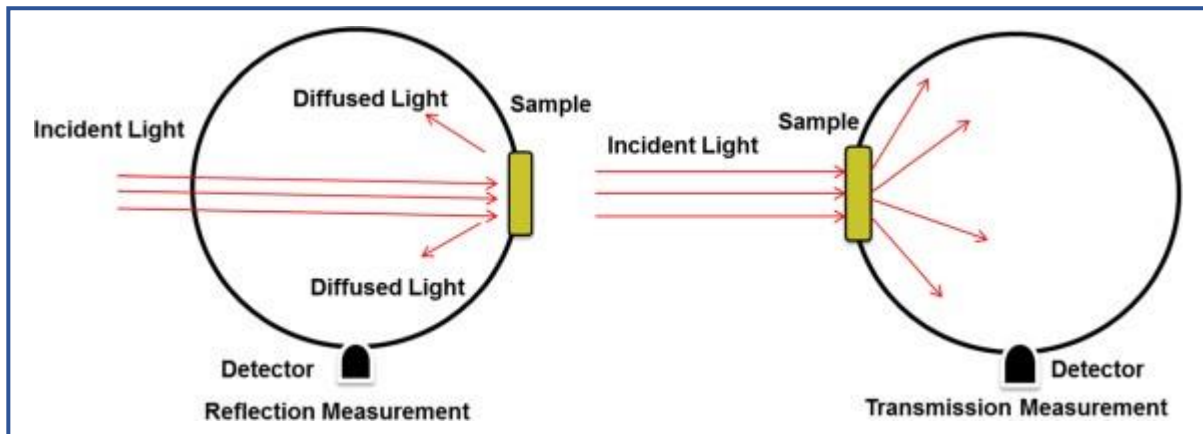
Fig.II.10 Total diffuse reflectance and transmittance measurement using the integrating sphere [24].

- **Film thickness**

The film thickness (d) is significant because it is a key factor influencing the electrical and optical characteristics of the film [25]. For the determination of the film thickness we usedthe method proposed by Swanepoel, which hinges on the use of the interference fringes of the transmittance of the elaborated nano-films [26]. Equation implies that the thickness is given by:

$$d = \frac{\lambda_1 \lambda_2}{2(\lambda_1 n_2 - \lambda_2 n_1)} \qquad \text{(II.10)}$$

Where λ_1 and λ_2 are the wavelengths at which two successive maxima or minima occur

and n_1 and n_2 are the corresponding refractive indices, n_1 and n_2 are derived from therelationship**:**

$$n_{1,2} = (N_{1,2}{}^2 + (N_{1,2} + S^2)^{0.5})^{0.5} \qquad \text{(II.11)}$$

Where S is the refractive index of glass and $N_{1,2}$ may be computed using the relationship[26]:

$$N_{1,2} = \frac{2S(T_M - T_m)}{T_M T_m} + \frac{S^2 + 1}{2} \qquad \text{(II.12)}$$
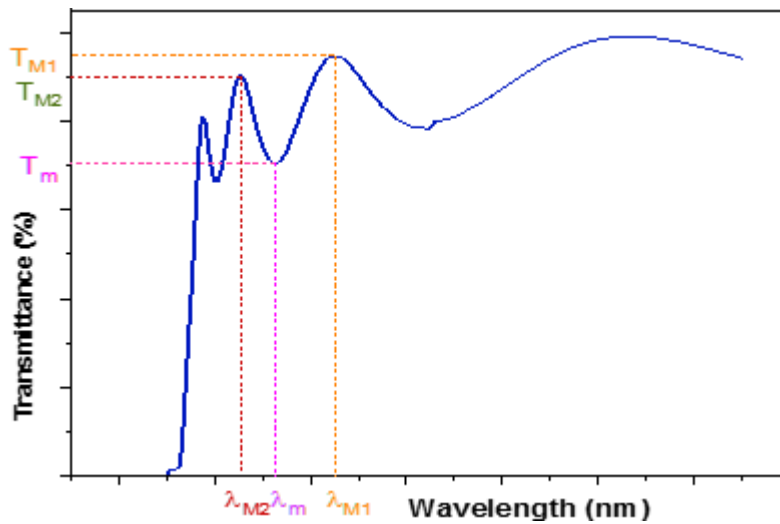
Fig.II.11 Method of interference fringes to determinate the thickness.

- **Absorption coefficient**

In the spectral domain where the light is absorbed, and knowing the thickness of the strong absorption layer as a function of the wavelength. We then define the optical gap Eg. According to the Beer-Lambert law [25]:

$$\alpha = \frac{1}{d} ln\frac{1}{T} \qquad \text{(II.13)}$$

Where: d: the thickness of the sample, T: measured transmission.

- **Band gap energy**

The optical energy band gaps Eg of the films were calculated using the Tauc's relationship as follows:

$$(\alpha \, hv)^n = A \, (hu - E_g) \qquad \text{(II.14)}$$

Where: α is absorption coefficient, A is constant, h is Planck's constant υ is photon frequency and n is ½ (Fig.II.12) or 2 for allowed direct, allowed indirect band gap semiconductors [27].
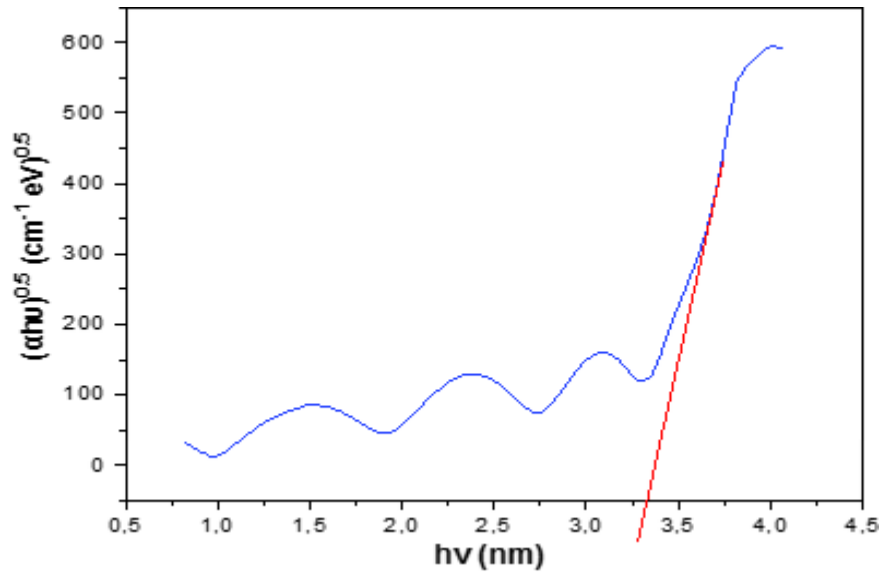
Fig.II.12 Determination of the indirect energy gap by the extrapolation method.

- **Urbach energy**

    The variation of the absorption coefficient with the Urbach energy is given by thefollowing equation:

$$\alpha = \alpha_0 \exp\left(\frac{hv}{E_u}\right) \qquad \text{(II.15)}$$

where α_0 is a constant and Eu is the Urbach energy. By plotting ln α as a function of hv (Fig.II.13), we can access the determination of the value of E_u [28]:

$$Ln \, \alpha = Ln\alpha_0 + \frac{hv}{E_u} \qquad \text{(II.16)}$$
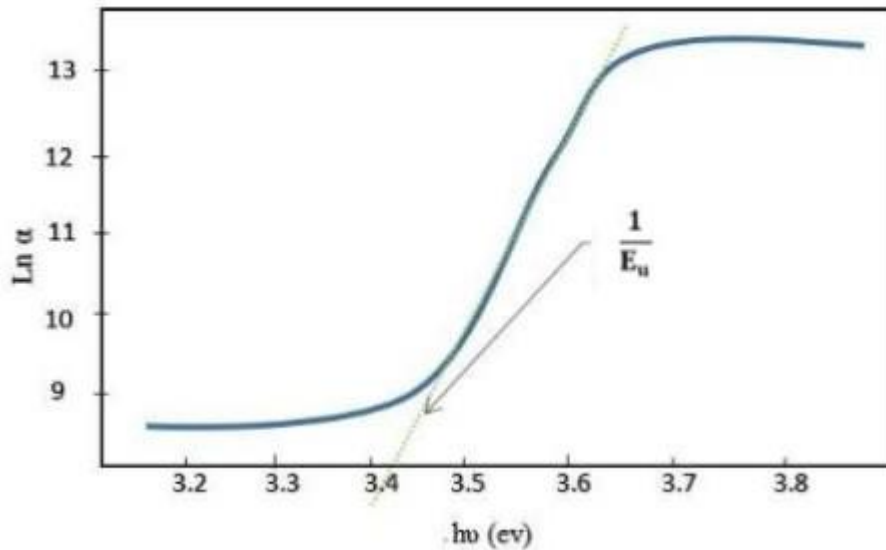
Fig.II.13 Determination of Urbach energy [7].

II.3.3. Four-point probe method

our-point probe measurer (FPP) is a tool that is frequently used to measure the resistivity value of a layer of an electronic material, specifically semi-conductor material used in electronic devices like silicon (Si), germanium (Ge), and gallium arsenide (GaAs). This measurer, which has four probes, uses two of them to measure electric current and the other two to measure voltage when they are introduced to the material (a sample). It is necessary to measure the resistivity value for a specific area and thickness in order to assess and review the material's qualities (Fig.II.14). Knowing the type of doping of a semi-conductor material (positive and negative) and the electronic mobility of a material are two more parameters that may be determined from material measurement utilizing this instrument [29].
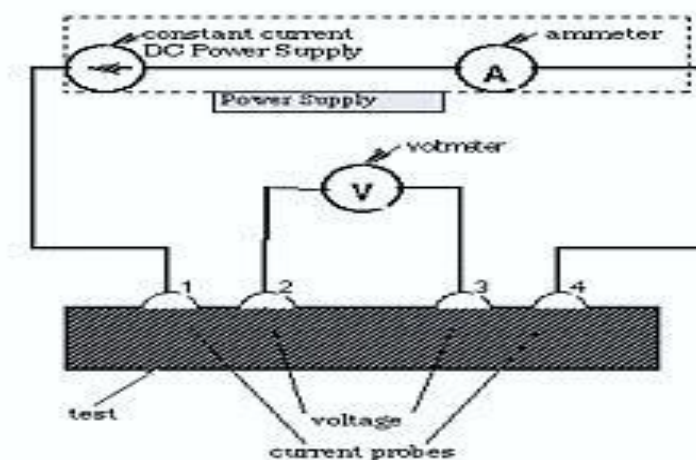
Fig.II.14 Four-point Circuit [29].

The resistivity of thin films was calculated according to the equation [30]:

$$\rho = R_s . d \qquad (II.17)$$

Where ρ is the resistivity, R_s is the square resistance ($R_s = (\frac{\pi.U}{ln2.I})$, U is the voltage and I is the current) and d is the film thickness. Based on previous considerations, we deduce the formula to calculate the conductivity:

$$\sigma = \frac{1}{\rho} \qquad (II.18)$$

II.3.4. Scanning Electron Microscopy (SEM)

Images of nanoscale resolution and a magnification of over 3 million can be created with SEM. It is one of the most used characterization approaches in nanofabrication because of this. Because electrons rather than light are employed to create an image, SEM has a high level of resolution. The Rayleigh criteria, which demonstrates that the distance between two independently resolvable spots is exactly proportional to the wavelength of the light utilized to generate the image, limit the resolution of a microscope (Fig.II.15). A photon of light has a wavelength that is nearly 100 times longer than that of an electron, which is dependent on energy. These field or thermionic emission-produced electrons are accelerated toward the sample by an anode in a high vacuum. The accelerating voltage can be used to regulate the resolution because the wavelength of an electron relies on its energy [31].
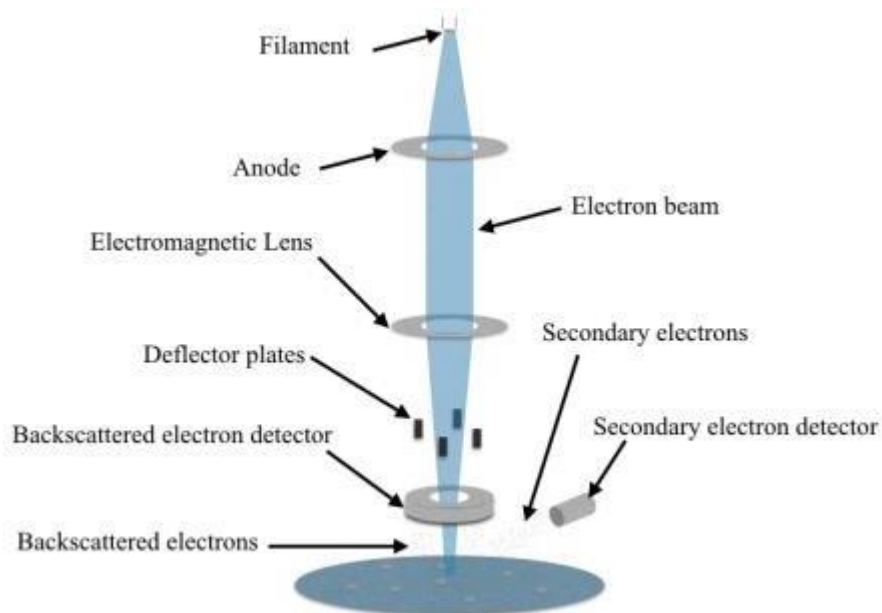
Fig.II.15 A schematic of the main components of a scanning electron microscope [31].

References

[1] **R. Amari**, « Etude de l'effet de dopage sur les propriétés physiques et chimiques des semiconducteurs à base d'oxyde synthétisées par la technique sol-gel spin coating », thèse de doctorat, université de M'sila, (2020).

[2] **K. Latrous, O. Berkani**, « Elaboration et caracterisation de couches minces d'oxyde de titane par la methode sol-gel », thèse de doctorat, université de Constantine, (2017).

[3] **A. Abdlekrim**, « Optimisation des conditions d'élaboration des couches minces d'oxyde d'étain SnO_2 par spray », thèse de doctorat, université de Biskra, (2016).

[4] **O. Daranfed, M. S. Aida,** « Elaboration et caractérisation des couches minces de Sulfure de Zinc préparées par spray ultrasonique », mémoire de magister, Université de Constantine, (2017).

[5] **A. Hafdallah, N. Attaf,** « Étude du dopage des couches minces de ZnO élaborées par spray ultrasonique », mémoire de magister, Université de Constantine, (2017).

[6] **R. Pérez-García**, « Controlled deposition of fullerenes: effects of topological nano-modifications of a surface on aggregation and growth phenomena », doctoral dissertation, Technische Universität Berlin, (2018).

[7] **C. Khelifi**, « Tin dioxide SnO_2 thin films deposited by ultrasonic spray technique: Properties and Applications», doctoral dissertation, University of Biskra, (2018).

[8] **R. Shwetharani, H. R. Chandan, M. Sakar, G. R. Balakrishna, K. R. Reddy**, Raghu, Photocatalytic semiconductor thin films for hydrogen production and environmental applications, International Journal of Hydrogen Energy, 45(36), pp 18289-18308.

[9] **M. Maache,** «Elaborattion de films Minces d'oxydes Semiconducteurs Par Voie sol-Gel»، doctoral dissertation, university of Biskra, (2014).

[10] **M. Attallah, R. Bensaha**, « Elaboration et caractérisation des couches minces d'oxyde de silicium obtenues par voie sol gel », mémoire de magister, Université de Constantine, (2017).

[11] **F. Medjaldi, A. Bouabellou**, « Préparation et caractérisation de couches minces d'oxyde de titane (TiO_2) et du couple d'oxydes (TiO_2/SnO_2) », mémoire de magister, université de Constantine, (2017).

[12] **M. C. Benachour, R. Bensaha**, « Elaboration et caractérisation des couches minces de TiO$_2$ dopées à l'erbium, à différentes températures et épaisseurs », mémoire de magister, université de Constantine, (2017).

[13] **S. Abbad**, « Etude de l'effet du dopage et des parametres de synthese de poudres nanocristallines de TiO$_2$ preparees par sol-gel sur les proprietes physiques et photo-catalytiques », doctoral dissertation, Université d'Oum El Bouaghi, (2022).

[14] **A. Boutelala, M. Mahtali,** « Elaboration et caractérisation de couches minces de TiO$_2$ Dope », mémoire de magister, université de Constantine, (2017).

[15] **H. Dehdouh, R. Bensaha**, « Propriétés physico-chimiques des couches minces de l'oxyde de titane. Effet de la concentration », mémoire de magister, université de Constantine, (2017).

[16] **J. Puetz, M. A. Aegerter**, Dip coating technique, Sol-gel technologies for glass producers and users, pp 37-48.

[17] **M. D. Tyona**, A theoritical study on spin coating technique, Advances in materials Research, 2(4) (2013), pp 195.

[18] **R. G. Larson, T. J. Rehg**, Spin coating, Liquid Film Coating: Scientific principles and their technological implications, (1997), pp 709-734.

[19] **N. Sahu, B. Parija, S. Panigrahi**, Fundamental understanding and modeling of spin coating process: A review, Indian Journal of Physics, 83(4) (2009), pp 493-502.

[20] **S. Fatimah, R. Ragadhita, D. F. Husaeni, A. B. D. Nandiyanto**, How to calculate crystallite size from x-ray diffraction (XRD) using Scherrer method, ASEAN Journal of Science and Engineering, 2(1) (2022), pp 65-76.

[21] **Y. Benkheta**, « Elaboration and characterization of thin layers of zinc oxide (ZnO) deposited by ultrasonic spray for photovoltaic and optoelectronic applications », doctoral dissertation, university of Biskra, (2019).

[22] **A. Attaf, A. Derbali, H. Saidi, M. S. Aida, M. Poulain**, the effect of ultrasonic wave amplitude on the physical properties of zinc oxide (ZnO) deposited by ultrasonic spray method, Materials Science and Engineering: B, 275(2022), pp 115525.

[23] **N. Karnakar, H. Ramana, P. Amani, D. S. Tharun, S. B. Sharma**, Analytical method development and validation of diclofenac sodium by UV-visible spectroscopy using AUC method, Spectroscopy, 2(2020), pp 3.

[24] **O. Hamdy, H. S. Mohammed**, Investigating the transmission profiles of 808 nm laser through different regions of the rat's head, Lasers in Medical Science, 36(4) (2021), pp 803-810.

[25] **F. Zeribi, A. Attaf, H. Saidi, L. Benmebrouk, M. S. Aida, H. Ezzaouia**, Dependence of the physical properties of titanium dioxide (TiO_2) thin films grown by sol-gel (spin-coating) process on thickness, ECS Journal of Solid State Science and Technology, 11(2) (2022), pp 023003.

[26] **K. Bedoud, H. Merabet, R. Graine**, Propriétés Optique de TiO_2 et Application de la Méthode de Swanepoel pour la Détermination de l'Épaisseur Optique et de l'Indice de Réfraction. Swanepoel, (2018).

[27] **A. amel guettaf,** « L'effet du dopage par l'étain sur les propriétés des couchesminces de TiO_2 élaborées par voie sol-gel (sping-coating), », mémoire de master, université de Biskra, (2017).

[28] **H. Meddas,** « Effet du dopage par l'azote sur les propriétés des films minces de dioxyde de titane préparés par procédé sol gel (spin coating) », mémoire de master, université de Biskra, (2020).

[29] **R. S. Waremra, P. Betaubun**, Analysis of electrical properties using the four-point probe method, In E3S Web of Conferences, 73(2018), pp 13019.

[30] **A. Attaf, A. Derbali. H. Saidi, H. Benamra, M. S. Aida, L. Derbali**, Physical properties of Pb doped ZnS thin films prepared by ultrasonic spray technique, Physics Letters A, 384(26) (2020), pp126199.

[31] **A. B. Dahlin, J. O. Tegenfeldt and F. Höök**, Improving the Instrumental Resolution of Sensors Based on Localized Surface Plasmon Resonance, Analytical Chemistry, 78(13)(2006), pp 4416-4423.

Chapter III

Experimental procedures, results and discussions

In this chapter, we presented the results of our work concerning the elaboration and characterization of Titanium dioxide thin films doped with different concentrations of Cesium (TiO$_2$: Cs), and deposited by the sol gel technique (spin coating). Then, we analyzed the obtained results for the purpose of studying the influence of Cesium ions doping on the structural, optical, electrical and photocatalytic properties of TiO$_2$ thin films.

III.1. Experimental details

III.1.1. Preparation of the substrate

III.1.1.1. Choice of substrate

The studied films were deposited on industrial glass substrates with a square surface (2.5 x 2.5) cm^2 and a thickness equal to 1.2 mm, cut with a diamond-tipped pen (Fig.III.1):

Fig.III.1 Glass substrates and diamond-tipped pen.

The choice of substrates is dictated by the physico-chemical properties of the substrate/material pair to be deposited. In our work, we chose glass slides as substrates for the following reasons:

- ✓ The glass has a greater softening temperature than the heat treatment temperature that our films underwent after deposition, and it has a thermal expansion coefficient that is comparable with that of the material that was deposited, limiting the effects of strains during annealing [1].
- ✓ For their transparency which adapts well for the optical characterization of films in the visible one [2].
- ✓ The glass substrates are transparent and insulating which allows a good optical and electrical characterization of our films [1].
- ✓ For economic reasons.

III.1.1.2. Cleaning of the substrate

To get good results, the substrates must be cleaned before the deposition. In fact, the substrate's surface condition has a significant impact on the properties of the deposited films, particularly on their uniformity and adherence.

Each substrate's surface needs to be cleaned to get rid of the many pollutants that are on it, and then it needs to be visually inspected for cleanliness. The substrate surfaces are cleaned in the manner described below:

1.Rinse with distilled water.	2.Cleaning with acetone for 5 min to remove grease.	3.Rinse with distilled water for 5 min.	4.Cleaning with alcohol for 5 min.	5.Rinse with distilled water for 5 min.	6.Drying using a dryer.
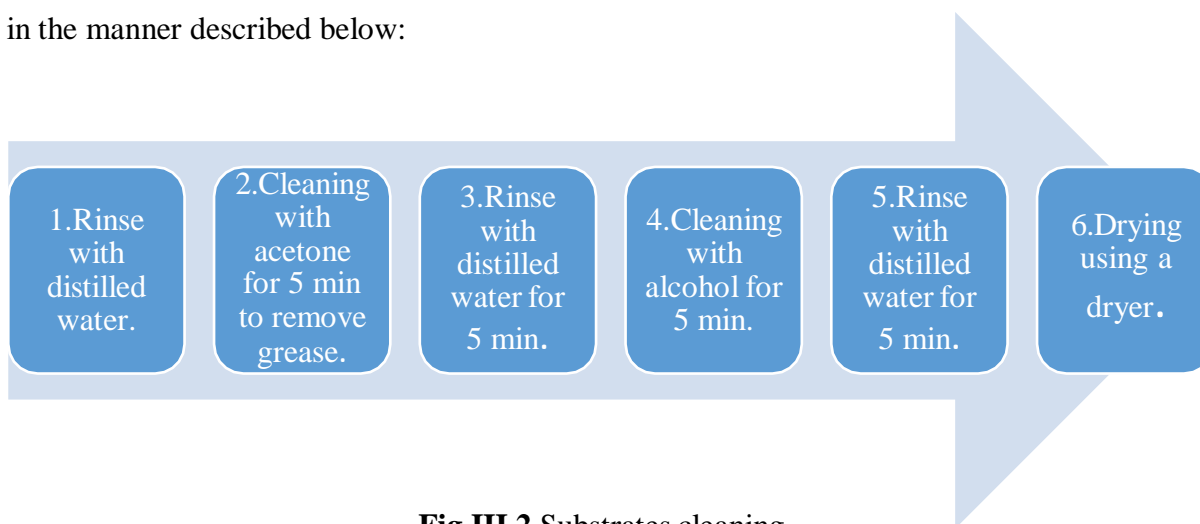
Fig.III.2 Substrates cleaning

III.1.2. Preparation of the solution

For the preparation of the deposition solution with a concentration of 0.2 mol/l, titanium tetra-isopropoxide (TTIP) used as precursor is dissolved in ethanol with acetylacetone, Cesium chloride (CsCl) was used as a doping source at (0, 0.5, 1, 1.5, 2 at%). The resulting mixture is stirred with a magnetic stirrer at a temperature equal to 50° C for 3 hours. The molar ratio of acetylacetone (stabilizer) and TTIP is equal to 1. The final solution is transparent yellowish in color and slightly viscous (Fig.III.3):

Fig.III.3 The deposit solution.

All the products which used during the preparations of our samples are presented in Table.III.1 with their different physico-chemical properties:

Table.III.1 Different properties of the used products.

Product	Formula	Molar mass (g / mol)	Density (g / cm^3)	Purity %	Boiling temperature (°C)	Utilisation
Titanium tetra isopropoxide	Ti [OCH(CH$_3$)$_2$] $_4$	284.23	0.96	95	232	precursor
Acetylacetone	CH$_3$COCH	100.12	0.97 at 20 °C	99.50	140.40	catalyst
Ethanol	C$_2$H$_5$OH	46.07	0.79 at 20 °C	96	78.37	solvent
Cesium chloride	CsCl	168.36	3.98	99.90	1297	doping precursor

III.1.3. Depositing of thin films

The preparation of the substrates and the solution is followed immediately by the deposition process. Spin coating technique was used to coat the films. We employed a machine called "Holmarc spin coater", which has the following shape and characteristics (Fig.III.4):
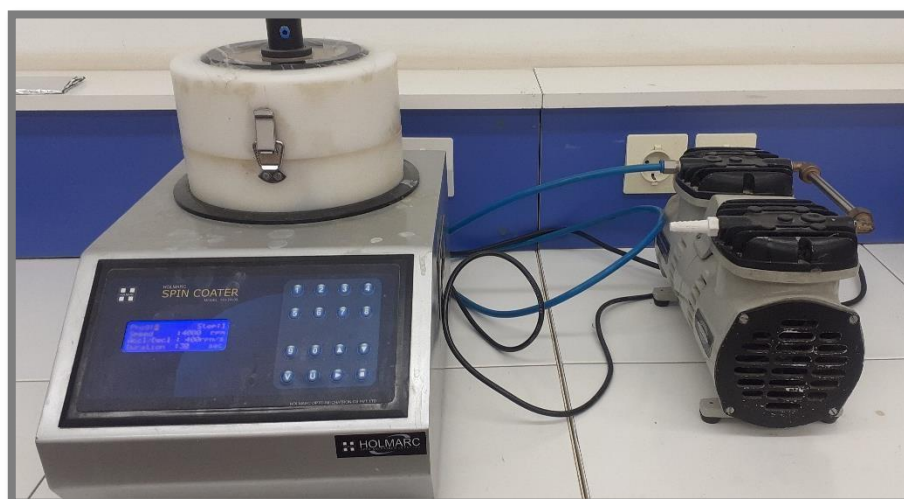
Fig.III.4 Holmarc Spin coater.

The previously specified precursor solution was poured onto the glass substrate until it covered the entire surface (V= 0.20 ml is the recommended amount). The substrate was rotated using the spin coater which reached 4000 rpm and stayed there for 30 seconds. The coated film was dried at 250 °C for 10 minutes after each coating. In order to start the production and crystallization of the TiO_2 thin film as well as the evaporation of organic solvents, a preheat treatment temperature of 250 °C is necessary. Following the five layer's depositions and drying,the resulting thin films were placed in a furnace and annealed at 600°C for two hours. The thin film deposition procedure is illustrated in the following diagram (Fig.III.5):
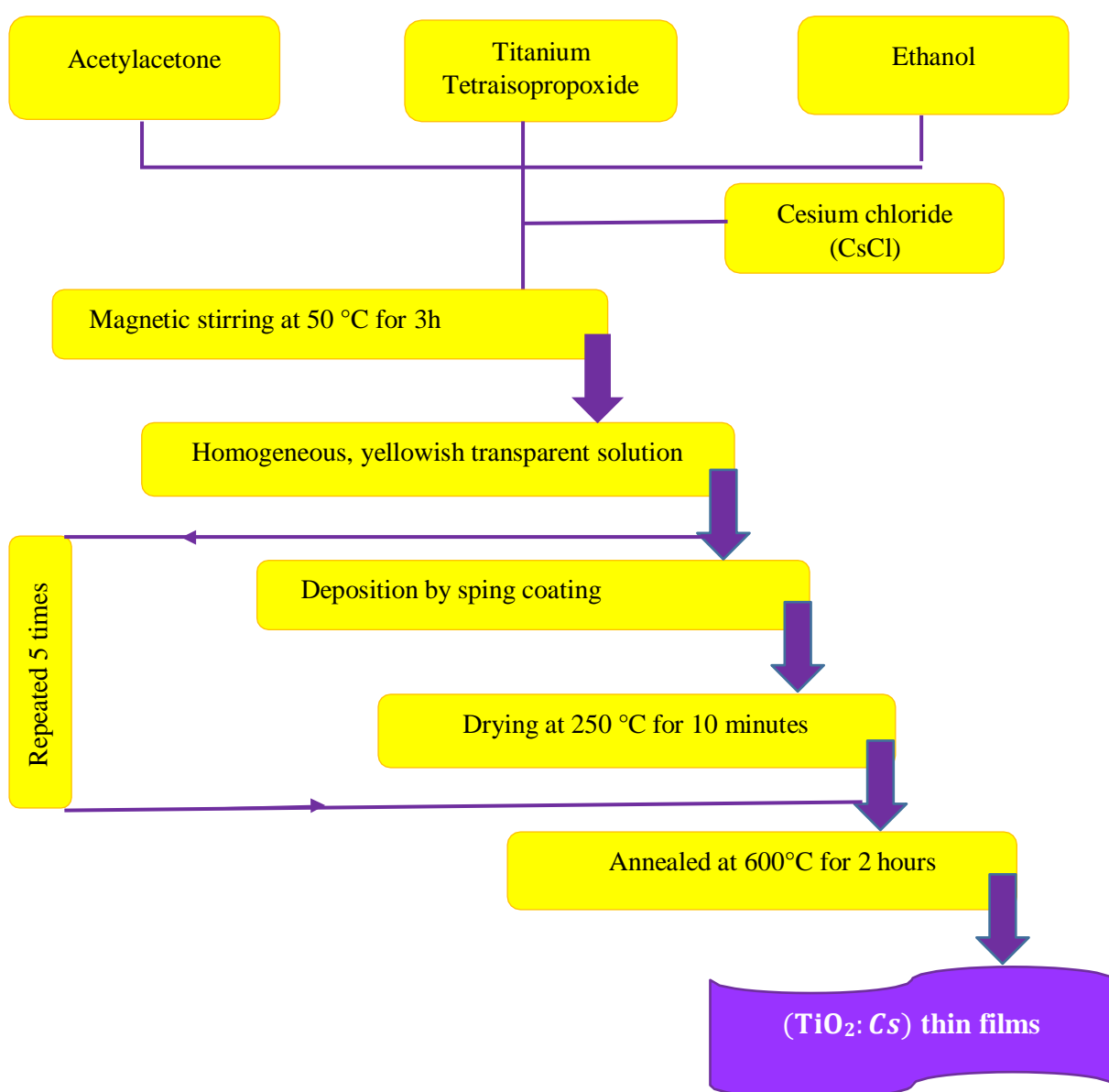
Fig.III.5 Diagram showing the deposition steps of Cesium doped Titanium dioxide thin films.

III.2. Results and discussions

The results we have obtained were compared with those of many previous research.

III.2.1. Adhesion test

Adhesion is defined as the condition in which two surfaces are held together by valence forces, by mechanical anchoring, or by both together. Adhesion to the substrate is certainly the first attribute a film must possess before any of its other properties can be manifested or exploited [3]. The simplest and quickest qualitative measure of film or coating adhesion is tape test which we have done by applying an adhesive tape to the film surface of our samples and pulled off again (Fig.III.6). We noticed that our layer is well adhered to the substrate.
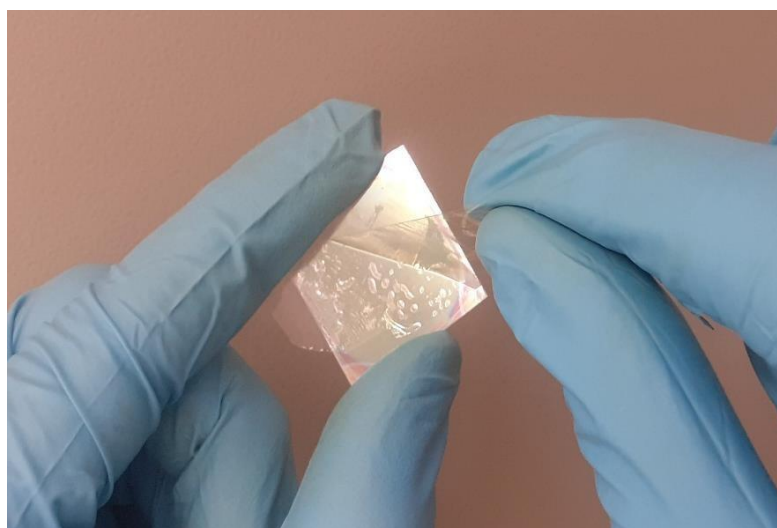
Fig.III.6 Simple adhesive tape tests.

III.2.2. Structural characteristics

III.2.2.1. X-ray diffraction

The crystallinity of our produced films was characterized by using X-ray diffraction method, using "RIGAKU MINIFLEX 600" diffractometer with CuK_α radiation ($\lambda = 1.54059$ Å). This technique makes it possible to obtain the diffractions presented in Fig.III.8. These diffractions are compared by the ASTM sheets (ICCD No. 21 -1272 for the anatase phase) (see Fig.III.7).
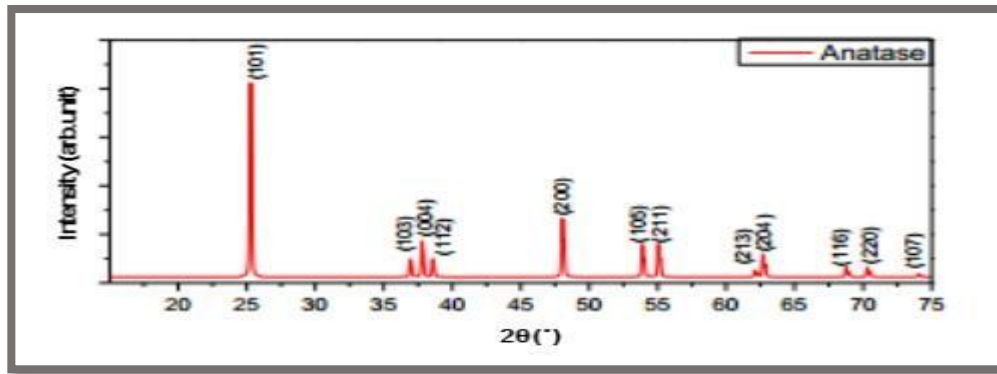
Fig.III.7 X-ray diffraction spectrum (the ASTM datasheet) of TiO_2 powder for anatase phase [4].

The x-ray diffraction pattern of TiO_2 thin films doped with different concentrations of Cesium (0, 0.5, 1, 1.5 and 2 at% Cs) deposited on glass substrates at annealing temperature (600℃) for two hours are shown in figure.III.8:
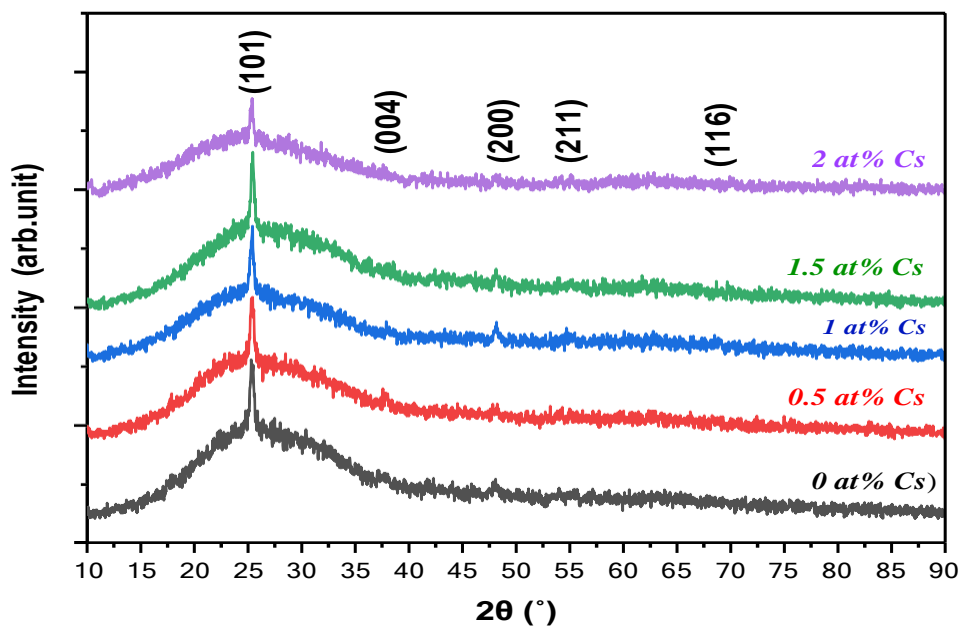
Fig.III.8 X-ray diffraction pattern of TiO_2 thin films doped with different concentration of Cesium.

From the comparison between the results obtained (Fig.III.8) and the ASTM sheet for TiO_2 (Fig.III.7), we can say that the films are oriented preferentially along to the plane (101) which corresponds to the diffraction angle about $2\theta=25.3°$, because this orientation has a minimum energy for the growth of our thin films. This result is in good agreement with the results of Boen Houng et al [5] and Y. Lu et al [6]. Also it is found that all the films are polycrystalline with a tetragonal crystal structure.

The XRD diffractions peaks around 2θ = 25.3°, 37.8°, 48°, 55° and 68.7° which correspond to the planes (101), (004), (200), (211) and (116) are in good agreement with those given in the ASTM sheets (ICCD No. 21 -1272) for anatanse phase [7].

The peak position, width and intensity are determined using Lorentz deconvolution of the most intense peak (101). The values of FWHM and peak intensities are added in the table below:

Table.III.2 The values of FWHM and peak intensities of (101) for (TiO$_2$: Cs) thin films with various concentration of cesium.

Cs (at%)	Intensity of the peak (101) (arb.unit)	FWHM (°)
0	121.66	0.44
0.5	114.80	0.39
1	105.07	0.36
1.5	127.27	0.38
2	65.96	0.31
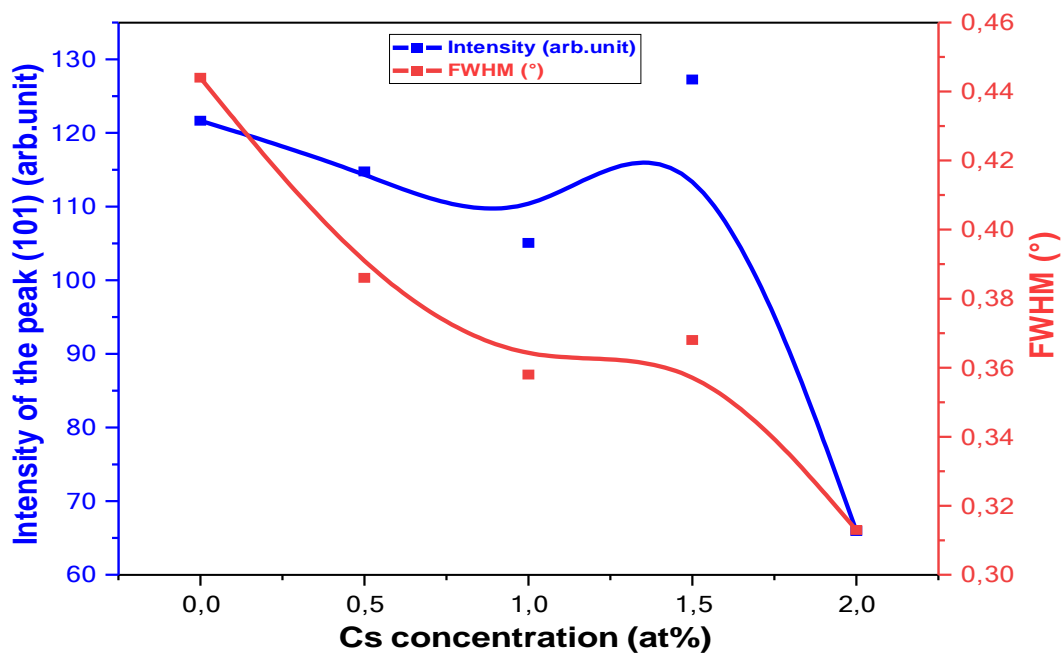
Fig.III.9 The variation of the most intense peak (101) and FWHM of (TiO$_2$: Cs) thin films at different Cs doping concentration.

➕ From Table.III.2 and Fig.III.9, it is observed that there is a narrowing in the line width of the peak with the increase in the Cs doping level, x-ray diffraction peaks get narrowing either. This narrowing might be due to the augmentation in the size of the crystallites [8]. In fact, the obvious decrease of the peak intensity (101) with increasing in Cs doping concentration can be attributed to the induced lattice disorder and the strain due the Cesium ions incorporation in TiO_2 lattice network [9].

III.2.2.2. Crystallite size, micro-strain and dislocation density

By exploiting the following relationships (Equation (II.7), (II.8) and (II.9)) which mentioned in chapter II, we estimated from the highest peak the crystallite size, micro-strain and dislocation density of the various samples. the results are illustrated in Table.III.3 and Fig.III.10:

Table.III.3 Crystallite size, micro-strain and dislocation density as a function of Cs concentration.

Cs (at%)	crystallite size (nm)	micro-strain ($\varepsilon \times 10^{-3}$)	Dislocation density ($\delta \times 10^{14}$) (line/m^3)
0	18.33	8.61	29.76
0.5	21.09	7.50	22.49
1	22.74	6.71	19.34
1.5	22.20	7.10	20.32
2	26.09	6.05	14.70
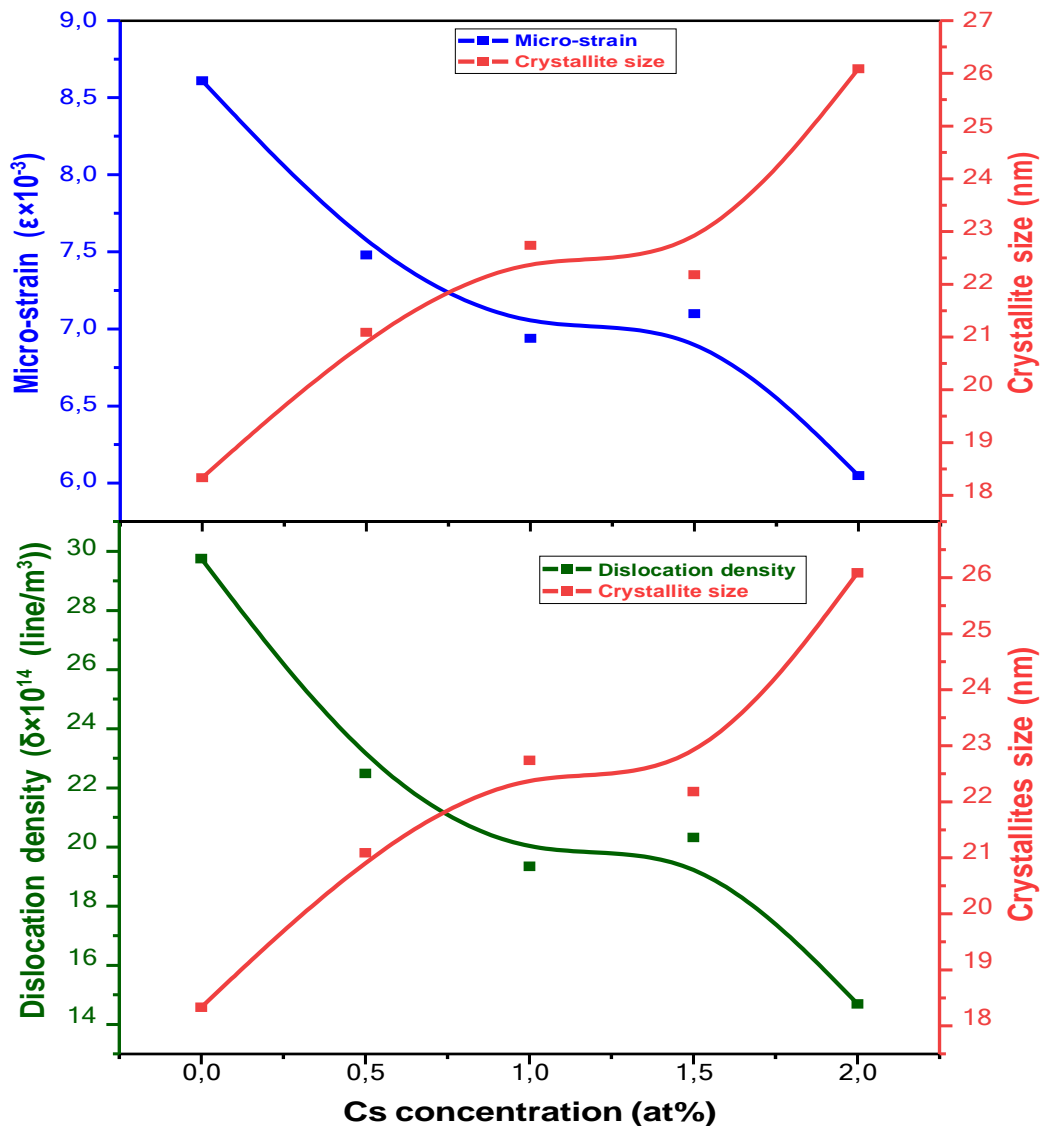
Fig.III.10 The variation of micro-strain and dislocation density with crystallite size as a function of Cesium doping concentration.

➤ It is easy to note from the figure above that crystallites size has an opposite behavior variation with both of micro-strain and dislocation density as a function of Cesium doping concentration.

➤ The crystallite size increased from 18.33 nm to 26.09 nm, while the micro-strain values decreased from 8.61×10^{-3} to 6.05×10^{-3}, with increasing of Cesium doping concentration. A similar result is also reported by Sheng Zhou et al [8]. The increase in crystallites size can be explained by the saturation of substitution sites and the excess of Cesium doping concentration occupying the interstitial sites in the structure [10].

In addition, the augmentation in the crystallite size may decrease the grain boundaries and this would lead to lower lattice defects in thin films resulting to decreases in micro-strain [8] while decreasing the dislocation density [10].

III.2.2.3. Lattice parameters

Anatase phase has a tetragonal structure with cell parameters were calculated using the following relation [11]:

$$\frac{1}{d_{hkl}^2} = \frac{h^2+k^2}{a^2} + \frac{l^2}{c^2} \qquad \text{(III.1)}$$

Where the interplanar spacing d_{hkl} is calculated by the law of Bragg and the most intense peak for Miller's indices are (101). Table.III.4 shows the experimental and theoretical cell parameters. It is noted that the results obtained are less than the theoretical cell parameters, which indicates the presence of compression in the cell, a similar result is also reported by A. Attaf et al [9] and A. Derbali et al [10].

Table.III.4 Experimental and theoretical cell parameters of (TiO_2: Cs) thin films.

Cs (at%)	2θ(°)	d_{hkl}(Å)	a= b (Å)	c(Å)	Reference parameter (ICCD card No. 21 -1272)
0	25.367	3.507	3.774	9.486	a_0(Å)= 3.785
0.5	25.371	3.506	3.773	9.484	c_0(Å)= 9.514
1	25.367	3.507	3.774	9.486	d_0(Å)= 3.520
1.5	25.423	3.499	3.766	9.465	
2	25.337	3.511	3.779	9.497	2θ (°) = 25.281

III.2.3. Optical properties

III.2.3.1. Transmittance and reflectance spectra

The reflectance and transmittance spectra of Cesium doped Titanium dioxide thin films are obtained by UV-visible spectroscopy as a function of wavelength over spectral range 300 –1500 nm (see Fig.III.11 and Fig.III.12):
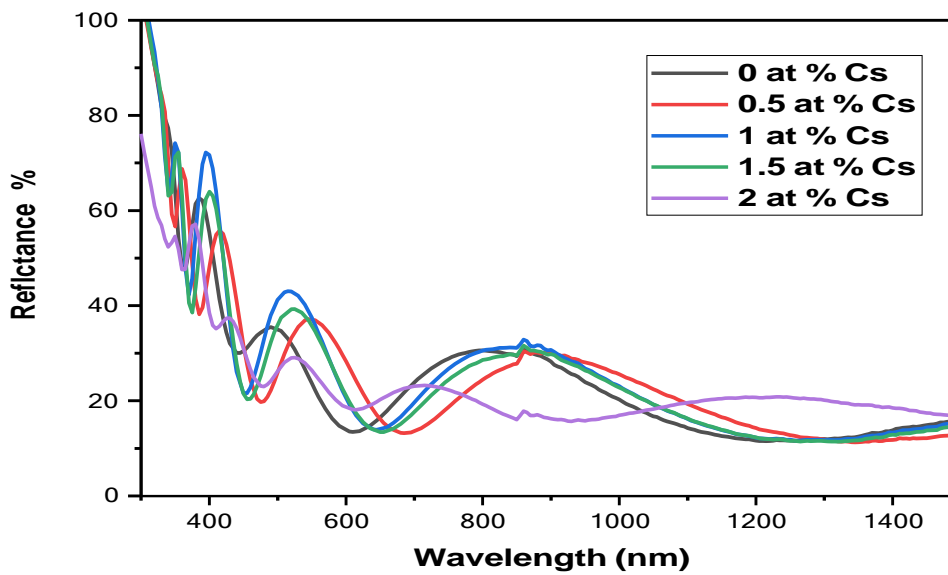
Fig.III.11 Reflectance spectra of (TiO_2: Cs) thin films with different doping concentration.
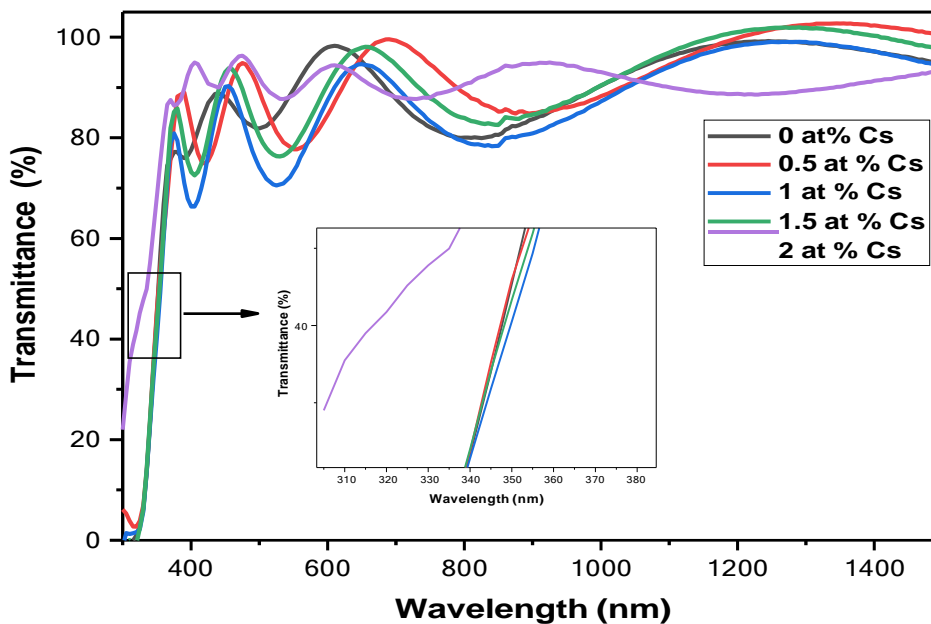
Fig.III.12 Transmittance spectra of (TiO_2: Cs) thin films with different doping concentration.

According to Fig.III.12 above, we can say that the spectra of transmittance is composed of two zones:

- A region of high transmittance in the wavelength range from 400 to 1500 nm. It is found that all the samples exhibit a high optical transparency about 80–92% in the visible range while the reflectance is found inside a confined interval (30–37) %.

Most of the samples show the presence of interference fringes in both reflectance and transmission spectra in the visible region, this can be attributed to the homogenous surface of the films, a similar result is also reported by Z. Chen et al [11].

- A region of strong absorption corresponds to the fundamental absorption ($\lambda < 400\ nm$). This zone related to the transition of the electron from the valence band (BV) to the conduction band (BC) [11], this last phenomenon is a very important characteristic for a semiconductor corresponding to the optical band gap energy (Eg) [12]. On the other hand, with increasing of Cesium doping concentration (from 0 to 1% at% Cs), the absorption edge of the deposited films was shifted towards the higher wavelength region (red shift), thereby reducing the band gap energy [11]. And for higher doping range (above 1% Cs at%), the absorption edge was shifted towards the lower wavelength region (blue shift), as a result, raising the band gap energy.

  - The significantly rise in the absorption edge for the sample of 2% at% Cs, is due may be to the reduction in the amplitude of the concerned interference fringes [11] which lead to the increase of its surface roughness [13].

  - In the low-wavelength side at 300 nm, the transmittance spectrum of the samples (2 at% Cs) does not cross the 0 point of the *y*-axis, most probably do not result in uniform coverage on the glass substrate, which is due to the formation of pinholes [14].

III.2.3.2. Optical gap and Urbach energy

The optical gap and disorder were estimated by the methods mentioned in chapter II (equation II.14 and II.16). Table.III.5 and Fig.III.13 shows the variation of indirect band gap and Urbach energy as a function of Cesium doping concentration.

Table.III.5 Indirect band gap and Urbach energies values as function of Cesium doping concentration.

Cs at %	0	0.5	1	1.5	2
Indirect band gap energy E_g(eV)	3.95	3.38	3.33	3.35	3.64
Urbach energy E_u (eV)	0.18	0.19	0.21	0.20	0.15
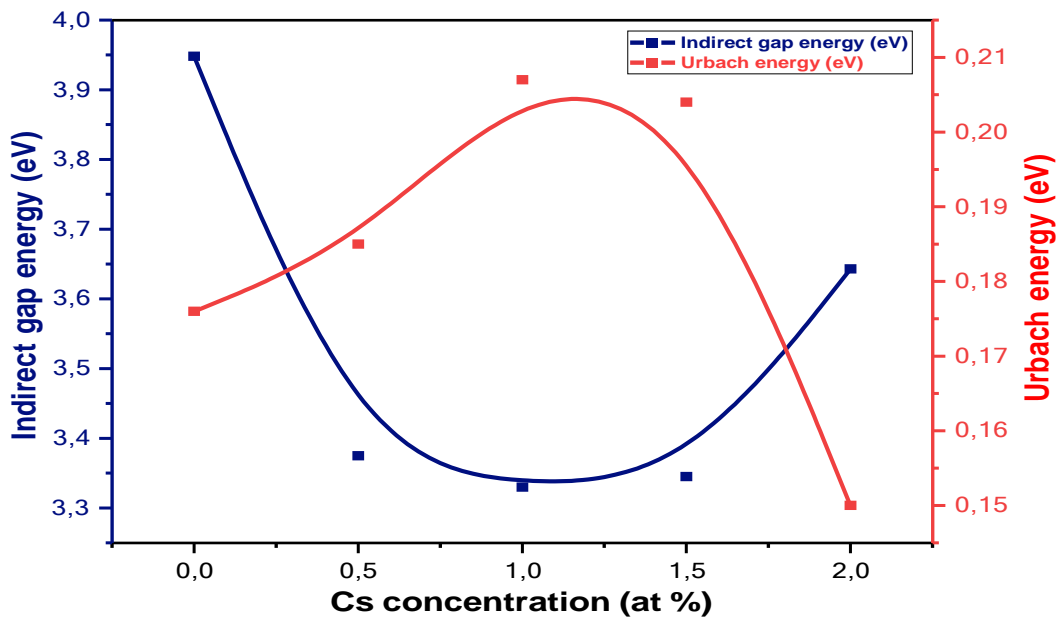
Fig.III.13 The variation of indirect band gap and Urbach energies as a function of Cesium doping concentration.

From table.III.5 and Fig.III.13, we noted that the indirect band gap and the Urbach energies are inversely aligned. The Urbach tail width or energy is used as signature of the disorder in the film network by Cesium doping concentration [16].

On the other hand, it can be seen that the indirect band gap is going through two ranges as a function of Cesium doping concentration:

- Low doping range from 0 to 1% at% Cs: It can be seen that depending on the increase in Cesium doping concentration, the indirect band gap values decreased from 3.95 eV up to 3.33 eV. This decrease can be attributed to the increasing of crystallites size as a function of the quantum confinement effect [17]. Fig.III.14 explains the relationship between gap energy and crystallites size.
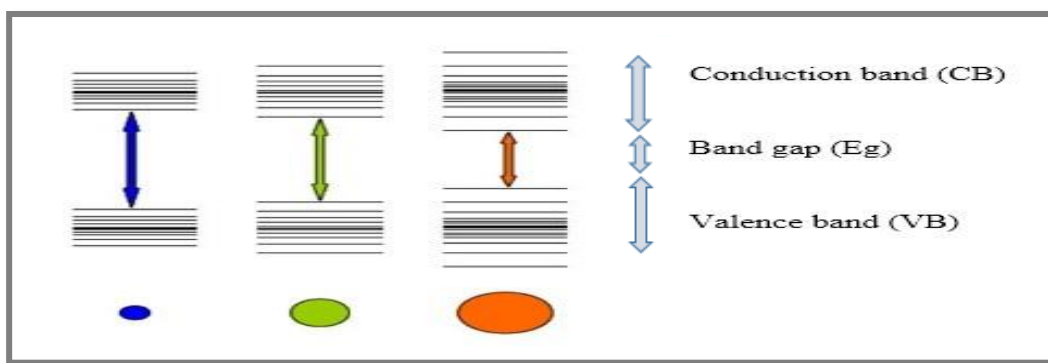
Fig.III.14 Diagram represented the relationship between crystallites size and band gap energy [1].

+ Higher doping range above 1% at% Cs: in this range, the indirect band gap values increased from 3.33 eV to 3.64 eV. The widening in band gap is attributed to Burstein-Moss effect as follows: carrier concentration is due to the high doping levels, fills blank states belonging to CB of the thin films so increases the energy magnitude necessary for the valence band to conduction band transitions [18]. In another way, based on Burstein-Moss effect, the increase in the carrier's density of semiconducting material due to Cesium doping causes a shift in the Fermi level and merges into conduction band which causes the low energy transition is obstructed. Thereby, a broadening in the indirect band gap [19]. This result is in good agreement with the results of Boean Houng et al [5], Aytaç GÜLTEKİN [20], Jakub Biedrzycki et al [15].

III.2.4. Thickness of the film

We calculate the film thickness (d) using the method of interference fringes (Swanepoel's method) which was mentioned in the second chapter (equation II.10), the obtained results are represented in the table below:

Table.III.6 Evolution of the thickness (d) with the Cesium doping concentration.

Cs at%	0	0.5	1	1.5	2
d (nm)	518	496	493	485	698

+ From 0 to 1.5 at% Cs, we note that the film thickness values are almost converging. So that, the effect of Cesium doping concentrations didn't significantly on film thickness, but it is clearly affected on the structure of our samples. Also, this convergence of values is reference to the sol gel technical (spin coating) which used in the samples preparation.

+ At a concentration of 2 $at\%$ Cs, the thickness values of the concerned sample increased due to measurement errors resulting from the interference fringes, which was inaccurate and unclear for this concentration (lack of interference fringes increases in account error of the film thickness), compared with other Cesium doping concentrations. On the other hand, the effect of Cesium doping on the structure is beginning to become clear in this concentration, which is explained by the lack of interference fringes.

III.2.5. Surface morphology

Cesium doping effect on the morphological properties of TiO$_2$ thin films were investigated by scanning electron microscopy (SEM), shown in Fig.III.15:
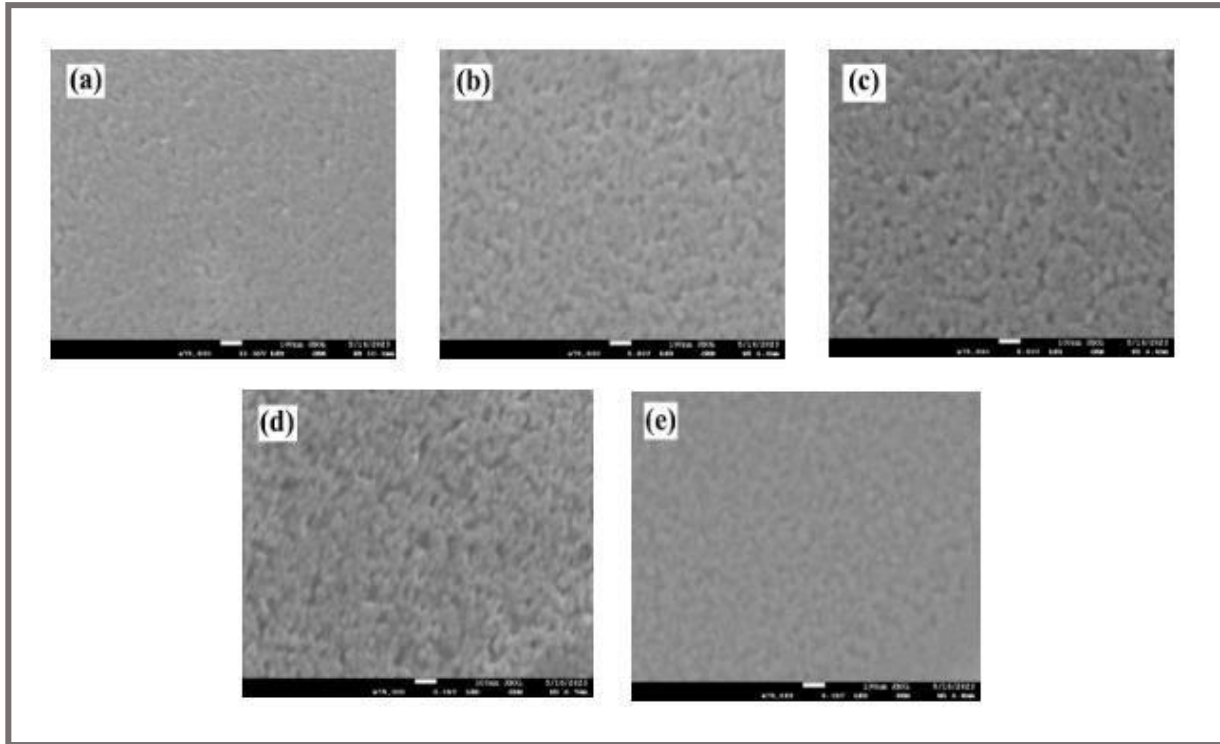
Fig.III.15 SEM surface images of (**a**) undoped, (**b**) 0.5 at%, (**c**) 1 at%, (**d**) 1.5 at% and (**e**) 2 at% of Cesium doped TiO$_2$ thin films.

As can be deduced from Fig.III.15, the obtained results show that the surface morphology of the different (TiO$_2$: Cs) thin films are homogeneous and is covered by pinhole grains with a disuniform distribution throughout the surface of the film especially in the sample of 2 $at\%$ Cs. Also, the crystallite size is increased as the concentration of Cs doping increased, which is corresponding with the results obtained from the XRD analysis. a similar result is also reported by N. Mohammadi et al [20].

III.2.6. Electrical properties

Using 4 point measurements that permit to indicate how $(TiO_2: Cs)$ films are resistive, the obtained results of electrical resistivity (ρ) and the conductivity (σ) as function of Cs doping concentration are showing in Table.III.7:

Table.III.7 Variation of conductivity and resistivity of $(TiO_2: Cs)$ with different doping concentration.

Cs at%	Resistivity (Ω cm)	Conductivity $(\Omega\ cm)^{-1}$
0	0.013	79.680
0.5	0.007	133.810
1	0.075	13.330
1.5	0.100	9.913
2	0.105	9.541

- From Table.III.7, one can observe that the values of the conductivity of our thin films are on order 10^1 and 10^2 (Ω cm) $^{-1}$. From 0 to 0.5 at% Cs, the conductivity increase from 79,680 $(\Omega\ cm)^{-1}$ to 133.810 $(\Omega\ cm)^{-1}$, then it decreases from 133.810 $(\Omega\ cm)^{-1}$ to 9.541 $(\Omega\ cm)^{-1}$ for (0.5 to 2 at % Cs). This change is may be due to the structure of the material and to make sure of this we need to use other characterization methods, XPS and Hall effect.

III.2.7. Photocatalytic studies

The photocatalytic activity of our samples was assessed initially by monitoring the degradation of methyl orange solutions irradiated with simulated UV-A solar light.

III.2.7.1. General characteristics of methyl orange dye

Methyl orange is a typical azo water-soluble anionic dye that is utilized in a variety of industries, including textile, printing, paper, pharmaceutical, food, and research labs [21,22]. Some properties of methyl orange are given in Table.III.8:

Table.III.8 General characteristics of methyl orange dye [21]	
Molecular structure	
Synonyms	Gold orange, Helianthine, Orange III
Molecular formula	$C_{14}H_{14}N_3NaO_3S$
Molar mass	$327.34\ g\ mol^{-1}$
Type	Anionic
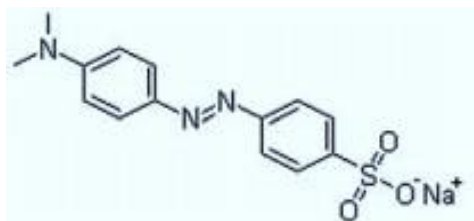
We chose methyl orange for the following reasons:

- ✓ It is a toxic organic dye.
- ✓ It does not degrade when exposed to light during photocatalytic experiment.
- ✓ Its structure is close to the structure of pollutants in the environment.

III.2.7.2. Photocatalytic degradation of methyl orange solution by (TiO_2: Cs) thin films

The methyl orange (MO) dye was selected as a model pollutant for the investigation of the photocatalytic activity of our TiO_2 films. MO solution was prepared by adding distilled water. (TiO_2: Cs) thin film was immersed in methyl orange solution inside glass bottles. After that, it was exposed to simulated UV-A solar light for one to six hours. The absorption of MO solution was measured by the UV-Visible spectra. Fig.III.16 below shows the methyl orange solution at different time irradiation:

Time
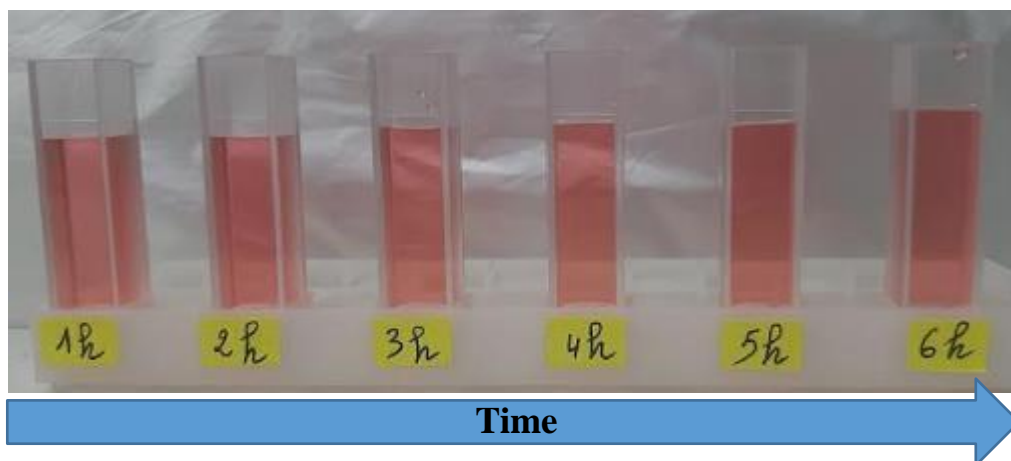
Fig.III.16 Photo degradation of MO blank solution exposed to UV-A simulated light for six hours.

- We note that the blank methyl orange solution does not degrade (very little decrease from 0.724 to 0.714) after exposure to UV-A simulated light for six hours, and this is evidence that it is not auto degradable.

➢ Fig.III.17 shows the absorption spectrum of the methyl orange solution in previous time periods:
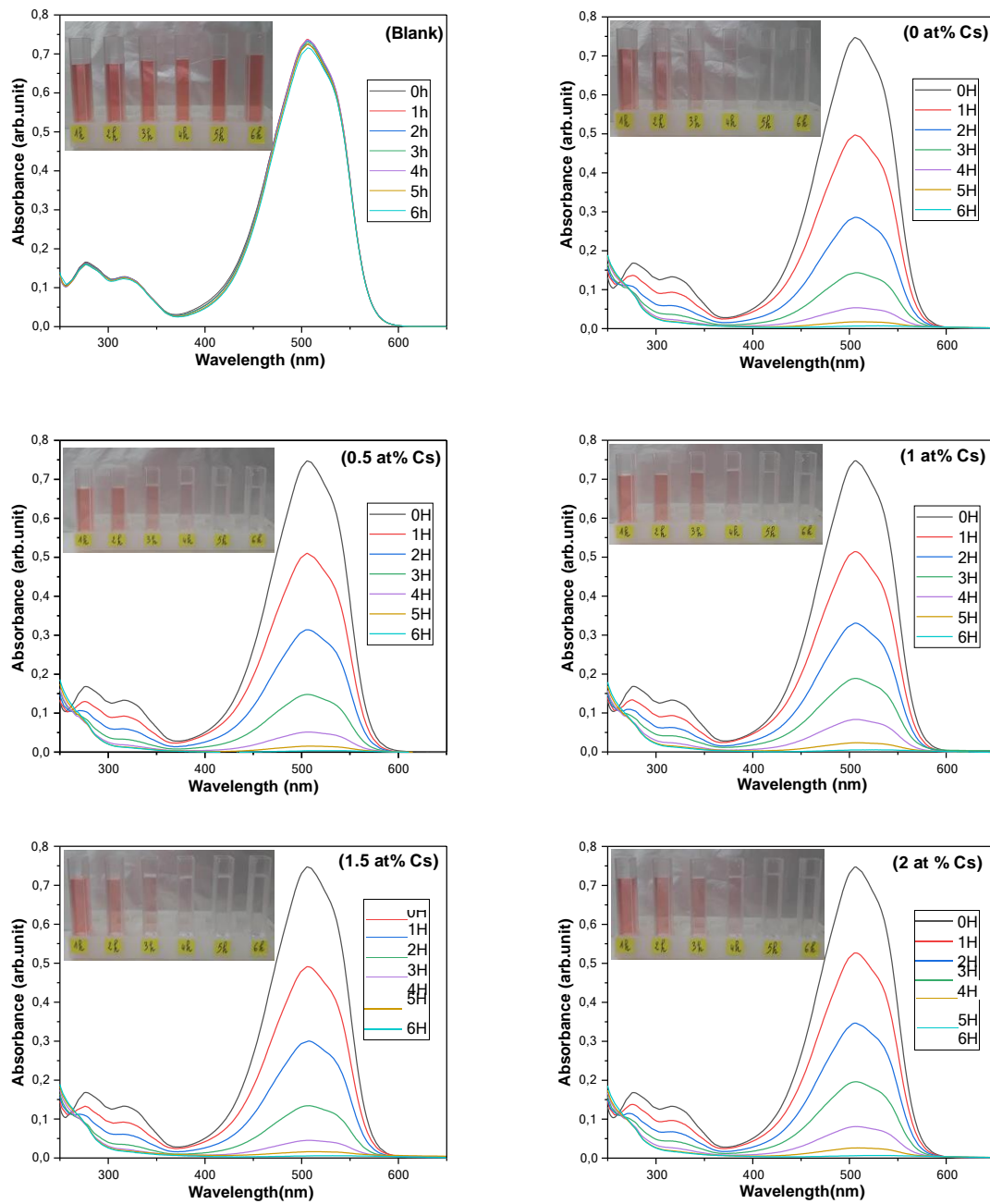
Fig.III.17 UV-Vis absorption spectra of MO solution exposed to UV-A simulated light for six hours.

According to Fig.III.17:

- A decrease in the height of the methyl orange peak is observed at the concerned wavelength of 507 nm. This decrease indicates that the thin layers of ($TiO_2 : Cs$) in the presence of UV-A simulated light for six hours are effective in degrading the methyl orange dye.

III.2.7.3. Photocatalytic reaction rate constant (K_{app})

Generally, the degradation kinetics of a compound follow the Langmuir-Hinshelwood model confirming the heterogeneous nature of the photocatalytic system. This model makes it possible to assess the rate of degradation of an organic pollutant at different concentrations [2].

The rate constant of MO photo degradation was studied by using pseudo-first-order kinetics which can be expressed as a given equation:

$$Ln\left(\frac{C_0}{C_t}\right) = K_{app}t \qquad \text{(III.2)}$$

Where C_0 is the dye concentration at time t = 0 min, C_t is the dye concentration at time t, t is irradiation time and K_{app} is the rate constant (see Fig.III.18).
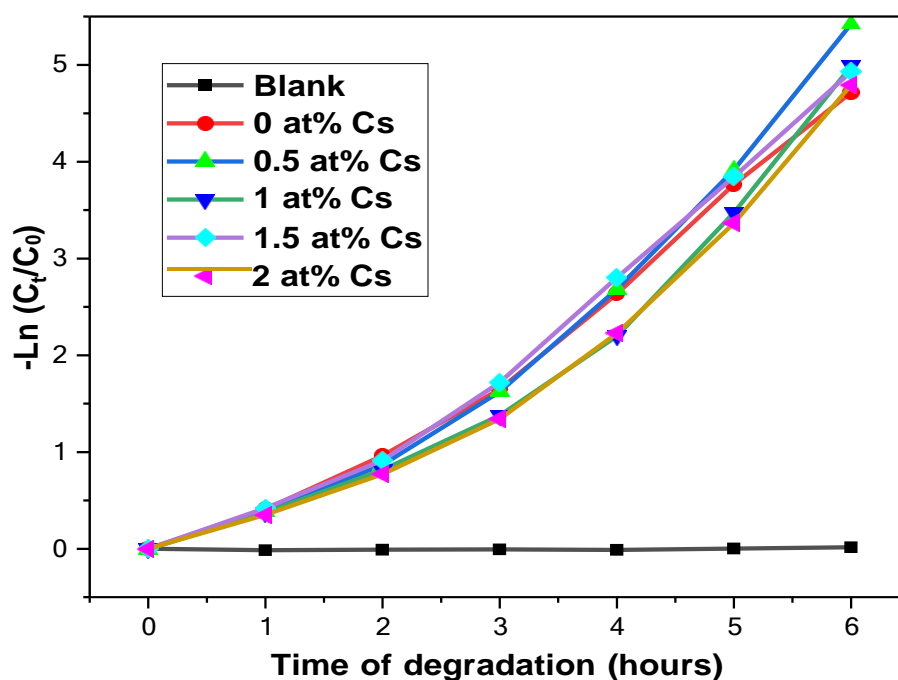
Fig.III.18 Plot of (-ln(C_t/C_0)) vs time irradiation over different Cesium doping concentration.

Table.III.9 Variation of K_{app} with Cesium doping concentration.

Cs (at%)	Blank	0	0.5	1	1.5	2
Kinetic constant (K_{app})(h^{-1})	0.003	0.804	0.898	0.804	0.513	0.781

✓ From Table.III.9, we noted that the highest value of kinetic constant is at 0.5 at% Cs. This indicates that the sample of 0.5 at% Cs has great efficacy in degrading the methyl orange dye compared with other Cesium doping concentrations.

General conclusion

The work presented in this study focused on the elaboration and characterization of Cesium doped Titanium dioxide TiO_2 thin films obtained by a sol-gel process (Spin-coating). The effect of doping on the structural, optical, electrical and photocatalytic properties of TiO_2 thin films was studied.

For this, a series of five samples were prepared and deposited on glass substrates at different doping rates from 0 to 2 at%. As starting materials, we used titanium tetra-isopropoxide (precursor), ethanol (solvent), acetylacetone (stabilizer) and Cesium chloride (source of dopant). The layers obtained are subjected to heat treatment (annealing) at 600°C. The results obtained showed that:

- $(TiO_2: Cs)$ thin films are well adhered to the substrate.
- Structural characterization by XRD shows that:

- The thin layers of $(TiO_2: Cs)$ obtained crystallized in the anatase phase with a preferential orientation along the (101) plane with the appearance of secondary orientations which indicating that the thin films are polycrystalline.
  The crystallite size increased with the increasing of Cesium doping concentration, and for this the micro-strain and the density of dislocations decreased. Cell compression occurred also.

- Optical characterization by UV-Visible spectroscopy shows that:

- All the samples exhibit a high optical transparency about 80–92% in the visible range while the reflectance is found inside a confined interval 30–37%.

- At a low doping range from 0 to 1% at% Cs, the indirect band gap values decreased from 3.95 eV up to 3.33 eV and for higher doping range above 1% at% Cs, the indirect band gap values increased from 3.33 eV to 3.64 eV.

- The indirect band gap and the Urbach energies are inversely aligned.

- The thin layers of $(TiO_2: Cs)$ in the presence of UV-A simulated light for six hours are effective in degrading the methyl orange dye.

- Most of $(TiO_2: Cs)$ thin films obtained converging thickness values.
- The morphological characterization by SEM shows that:

- the surface morphology of all the samples are homogeneous and dense.

- The electrical characterization of the films shows that:

- The values of the conductivity of our thin films is on order 10^1 and 10^2 $(\Omega\,\text{cm})^{-1}$.

From the results obtained, it can be said that the elaborate thin layers can be used in several applications such as photo-catalyst, optical window, gas sensors.

Our goals are to enhance the electrical characteristics of TiO_2 thin films so that they can be used in solar fields, for instance by applying co-doping or other types of doping.

References

[1] **R. Messemeche**, « Caractérisation de couches minces d'oxyde de titane (TiO2) Obtenues par Sol Gel (Spin coating) : L'effet de la concentration de la solution », mémoire de master, université de Biskra, (2016).

[2] **R. messemche**, « Elaboration and characterization of undoped and doped titanium dioxide thin layers by sol gel (spin coating) for photocatalytic applications », doctoral dissertation, université de biskra, (2021).

[3] **O. Benkhetta**, « Effet de la concentration de la solution sur les propriétés des couches minces de dioxyde de titane déposées par spray pyrolyse ultrasonique », mémoire de master, université de Biskra, (2019).

[4] **B.Houng, C.C.Liu, and M.T.Hung**, Structural , electrical and optical properties of molybdenum-doped TiO_2 thin films, Ceram. Int., 39(4) (2013), pp. 3669–3676.

[5] **Y. Lu et al**, Doping concentration effects upon column-structured $TiO_{2:}$ Nb for transparent conductive thin films prepared by a sol-gel method, J. Alloys Compd., 663(2016), pp. 413–418.

[6] **H. Benamra, H. Saidi, A. Attaf, M. S. Aida, A. Derbali, and N. Attaf**, Physical properties of Al-doped ZnS thin films prepared by ultrasonic spray technique, Surfaces and Interfaces, 21(2020), pp. 100645.

[7] **S. Chala**, « L'effet de dopage par l'aluminium sur les propriétés des couches minces du TiO_2 élaborées par voie Sol-Gel (spin caoting) », mémoire de master, université de Biskra, (2017).

[8] **O. Benkhetta et al**, Precursor concentration effect on the physical properties of transparent titania (Anatase-TiO_2) thin films grown by ultrasonic spray process for optoelectronics application,Optical materials, 132(2022).

[9] **A. Attaf, A. Derbali. H. Saidi, H. Benamra, M. S. Aida, L. Derbali**, Physical properties of Pb doped ZnS thin films prepared by ultrasonic spray technique, Physics Letters A, 384(26) (2020), pp126199.

[10] **A. Derbali et al**, Br doping effect on structural, optical and electrical properties of ZnS thin films deposited by ultrasonic spray, Mater. Sci. Eng. B Solid-State Mater. Adv. Technol., 268(2021), pp 115135.

[11] **Z. Chen, I.Dündar, I.Oja Acik, and A.Mere**, TiO_2 thin films by ultrasonic spray pyrolysis, IOP Conf. Ser. Mater. Sci. Eng., 503(1) (2019).

[12] **A. Yahia et al**, Structural, optical, morphological and electrical properties of indium oxide thin films prepared by sol gel spin coating process, Surfaces and Interfaces, (14) (2019), pp. 158–165.

[13] **A. Nakaruk, D. Ragazzon, and C.C.Sorrell**, Anatase thin films by ultrasonic spray pyrolysis, J. Anal. Appl. Pyrolysis, 88(1) (2010), pp 98–101.

[14] **I. Dundar, A.Mere, V.Mikli, and M.Krunks**, Catalysts Thickness Effect on Photocatalytic Activity of TiO_2 thin Films fabricated by Ultrasonic Spray Pyrolysis, (2020).

[15] **R. Messemeche et al**., Elaboration and characterization of nano-crystalline layers of transparent titanium dioxide (Anatase-TiO_2) deposited by a sol-gel (spin coating) process, Surfaces and Interfaces, 19, pp100482, 2020,

[16] **C. Khelifi, A. Attaf, H. saidi, A. Yahia, and M. Dahnoun**, Investigation of F doped SnO_2 thin films properties deposited via ultrasonic spray technique for several applications, Surfaces and Interfaces, 15(2019), pp. 244–249.

[17] **A. Badawi, M. G. Althobaiti, S. S. Alharthi, and A. M. Al-baradi**, Tailoring the optical properties of CdO nanostructures via barium doping for optical windows applications, Phys. Lett. A,(411)(2021), pp 127553.

[18] **A. Gültekİn**, Effect of Au Nanoparticles Doping on The Properties of TiO_2 Thin Films, 20(1) (2014), pp 10–14.

[19] **J. Biedrzycki , S.Livraghi, E.Giamello , S.Agnoli , G.Granozzi**, Fluorine- and Niobium-Doped TiO_2 : Chemical and Spectroscopic Properties of Polycrystalline n-Type-Doped Anatase (2023).

[20] **T.J.Webster**, Synthesis, characterization,and performance evaluation of multilayered photoanodes by introducing mesoporous carbon and TiO_2 for humic acid adsorption, (2016), pp 3969–3978.

[21] **F.Deniz**, Optimization of methyl orange bioremoval by Prunus amygdalus L. (almond) shell waste: Taguchi methodology approach and biosorption system design, Desalin. Water Treat., 51(37) (2013), pp 7067–7073.

[22] **N. Mohammadi, H. Khani, V. Kumar, E. Amereh, and S. Agarwal**, Journal of Colloid and Interface Science Adsorption process of methyl orange dye onto mesoporous carbon material – kinetic and thermodynamic studies, J. Colloid Interface Sci., 362(2) (2011), pp 457–462.

Annexe

Name and formula

Reference code: 1272-021-00

Mineral name: Anatase, syn
Compound name: Titanium Oxide
PDF index name: Titanium Oxide

Empirical formula: O_2Ti
Chemical formula: TiO_2

Crystallographic parameters

Crystal system: Tetragonal
Space group: I41/amd
Space group number: 141

a (?):   3,7852
b (?):   3,7852
c (?):   9,5139
Alpha (°):   90,0000
Beta (°):   90,0000
Gamma (°):   90,0000

Calculated   density   (g/cm^3):   3,89
Volume of cell (10^6 pm^3):   136,31
Z: 4,00

RIR: 3,30

Subfiles and quality

Subfiles: Alloy, metal or intermetalic
                                   Common Phase
                                   Corrosion
                                   Educational pattern
                                   Forensic
                                   Inorganic
                                   Mineral
                                   NBS pattern
                                   Pharmaceutical
                                   Pigment/Dye
Quality: Star (S)

Comments

Color: Colorless
Creation Date: 1970/1/1
Modification Date: 1970/1/1

Color:	Colorless
Additional Patterns:	See ICSD 9852 (PDF 01-071-1166)
Sample Source or Locality:	Sample obtained from National Lead Co., South Amboy, New Jersey, USA. Anatase and another polymorph, brookite (orthorhombic), are converted to rutile (tetragonal) by heating above 700 C. Pattern reviewed by Holzer, J., McCarthy, G., North Dakota State Univ, Fargo, North Dakota, USA, ICDD Grant-in-Aid .)1990(Agrees well with experimental and calculated patterns
Additional Patterns:	Validated by calculated pattern
Temperature of Data Collection:	Pattern taken at 25 C.

References

Primary reference:	Natl. Bur. Stand. (U.S.) Monogr. 25)1969(,82 ,**7** ,

Peak list

```
No.     h     k     l       d [A]      2Theta[deg]  I [%]
100,0    25,281   3,52000    1    0    1    1
10,0     36,947   2,43100    3    0    1    2
20,0     37,801   2,37800    4    0    0    3
10,0     38,576   2,33200    2    1    1    4
35,0     48,050   1,89200    0    0    2    5
20,0     53,891   1,69990    5    0    1    6
20,0     55,062   1,66650    1    1    2    7
4,0      62,121   1,49300    3    1    2    8
14,0     62,690   1,48080    4    0    2    9
6,0      68,762   1,36410    6    1    1    10
6,0      70,311   1,33780    0    2    2    11
2,0      74,031   1,27950    7    0    1    12
10,0     75,032   1,26490    5    1    2    13
4,0      76,020   1,25090    1    0    3    14
2,0      80,727   1,18940    8    0    0    15
2,0      82,139   1,17250    3    0    3    16
6,0      82,662   1,16640    4    2    2    17
4,0      83,149   1,16080    2    1    3    18
2,0      93,221   1,06000    7    1    2    19
4,0      94,182   1,05170    5    0    3    20
4,0      95,143   1,04360    1    2    3    21
2,0      98,319   1,01820    9    0    1    22
2,0      99,804   1,00700    8    0    2    23
2,0      101,221  0,99670    3    2    3    24
4,0      107,448  0,95550    6    1    3    25
4,0      108,963  0,94640    0    0    4    26
2,0      112,841  0,92460    7    0    3    27
2,0      113,861  0,91920    5    2    3    28
2,0      114,909  0,91380    1    1    4    29
4,0      118,439  0,89660    9    1    2    30
2,0      120,104  0,88900    8    2    2    31
2,0      121,725  0,88190    3    1    4    32
2,0      122,336  0,87930    4    0    4    33
2,0      131,036  0,84640    0    2    4    34
2,0      135,998  0,83080    7    2    3    35
4,0      137,391  0,82680    5    1    4    36
2,0      143,888  0,81020    9    0    3    37
4,0      150,039  0,79740    4    2    4    38
```

Effect of Cesium doping on the properties of Titanium dioxide thin films elaboratedby Sol-gel (Spin coating) and their photocatalytic applications.

Abstract:

In this study, we were prepared (TiO$_2$: Cs) thin films by Sol-gel (spin coating) technique onto glass substrates with doping percent varied from 0 at% to 2 at%. The influence of Cs doping on structural, optical, electrical and photocatalytic properties were investigated, then they were characterized using X-ray diffraction, UV-Visible spectroscopy, Scanning Electron Microscopy (SEM) and four-point probe method for electrical measurement. The obtained results show that the films are a polycrystalline nature with prefertional orientation along to (101) plane corresponding to anatase phase. The crystallite size of the films increased with the increasing of Cesium doping concentration. The optical analyses depict that the films have a high transmission in the visible range about 80–92%. Also, thin layers of (TiO$_2$: Cs) in the presence of UV-A simulated light are effective in degrading the methyl orange dye. In addition, the electrical measurements indicate that the resistivity of (TiO$_2$: Cs) thin films is on order 10^1 and 10^2 (Ω cm)$^{-1}$.

Keywords*:* Thin films, TiO$_2$, Cs, spin coating, doping, photocatalysis, methyl orange.

تأثير التطعيم بالسيزيوم على خواص الأغشية الرقيقة لثاني أكسيد التيتانيوم المحضرة بواسطة تقنية طلاء الدوران وتطبيقاتها التحفيزية الضوئية.

الملخص:

في هذه الدراسة تم تحضير شرائح رقيقة **TiO$_2$** غير المطعمة و المطعمة ب **Cs** باستخدام تقنية طلاء الدوران على ركائز زجاجية مع نسبة تطعيم تتراوح بين **0%** الى **2 %** . تمت دراسة تاثير هذا التطعيم على الخصائص البنيوية، الضوئية، الكهربائية و التحفيزية الضوئية من خلال توصيفها باستخدام حيود الاشعة السينية، التحليل الطيفي للاشعة فوق البنفسجية, المجهر الالكتروني الماسح و تقنية التلامسات الأربعة للدراسة الكهربائية. أظهرت النتائج المتحصل عليها ان الاغشية ذات طبيعة متعددة البلورات مع توجيه مفضل للنمو **(101)** وفق طور الاناتاز بالإضافة الى زيادة حجم البلورات مع زيادة تركيز التطعيم. كما توضح التحليلات الضوئية ان الشرائح لها نفاذية تتراوح بين **80 %** و **92 %**. أيضا ان شرائح أكسيد التيتانيوم المطعمة لها فعالية كبيرة في تفكيك صبغة الميثيل البرتقالي الر مركبات اقل خطرا على البيئة والصحة. وقد أظهرت الدراسات ان لهذه العينات ناقلية من رتبة **10^1** و **10^2** اوم-^{1} سم^1.

الكلمات المفتاحية: الشرائح الرقيقة، TiO2, Cs, تقنية طلاء الدوران، التطعيم، التحفيز الضوئي و صبغة الميثيل البرتقالي.

Effet du dopage au césium sur les propriétés des couches minces de dioxyde de titane élaborées par Sol-gel (Spin coating) et leurs applications photocatalytiques.

Résumé :

Dans cette étude, nous avons préparé des couches minces de (TiO$_2$: Cs) par la technique Sol-gel (spin coating) sur des substrats de verre avec un pourcentage de dopage variant de 0 at% à 2 at%. L'influence du dopage Cs sur les propriétés structurelles, optiques, électriques et photocatalytiques a été étudiée, puis elles ont été caractérisées à l'aide de la diffraction des rayons X, de la spectroscopie UV-Visible, de la microscopie électronique à balayage (MEB) et de la méthode de sonde à quatre points pour la mesure électrique. Les résultats obtenus montrent que les films sont de nature polycristalline avec une orientation préférentielle selon le plan (101) correspondant à la phase anatase. La taille des cristallites des films a augmenté avec l'augmentation de la concentration de dopage au césium. Les analyses optiques montrent que les films ont une transmission élevée dans le domaine visible d'environ 80 à 92 %. De plus, de fines couches de (TiO$_2$: Cs) en présence de lumière simulée UV-A sont efficaces pour dégrader le colorant méthyl orange. De plus, les mesures électriques indiquent que la résistivité des couches minces de (TiO$_2$: Cs) est de l'ordre de 10^1 et 10^2 (Ω cm)$^{-1}$.

Mots clés : Couches minces, TiO$_2$, Cs, spin coating, dopage, photocatalyse, methyl orange.